MATHEMATICS OF COMPUTATION
Volume 00, Number 0, Pages 000–000
S 0025-5718(XX)0000-0

A HIGHLY ACCURATE BOUNDARY INTEGRAL METHOD FOR THE ELASTIC OBSTACLE SCATTERING PROBLEM

HEPING DONG, JUN LAI, AND PEIJUN LI

Abstract. Consider the scattering of a time-harmonic plane wave by a rigid obstacle embedded in a homogeneous and isotropic elastic medium in two dimensions. In this paper, a novel boundary integral formulation is proposed and its highly accurate numerical method is developed for the elastic obstacle scattering problem. More specifically, based on the Helmholtz decomposition, the model problem is reduced to a coupled boundary integral equation with singular kernels. A regularized system is constructed in order to handle the degenerated integral operators. The semi-discrete and full-discrete schemes are studied for the boundary integral system by using the collocation method. Convergence is established for the numerical schemes in some appropriate Sobolev spaces. Numerical experiments are presented for both smooth and nonsmooth obstacles to demonstrate the superior performance of the proposed method. Furthermore, we extend this numerical method to the Neumann problem and the three-dimensional elastic obstacle scattering problem.

1. Introduction

The phenomena of elastic scattering by obstacles have received increasing attention due to the significant applications in diverse scientific areas such as geological exploration, nondestructive testing, and medical diagnostics [3, 21, 28]. There are many mathematical and computational results available for the scattering problems of elastic waves [1, 11, 22, 25, 27]. An accurate and efficient numerical method plays an important role in many of these applications. This paper is concerned with the scattering of a time-harmonic plane wave by a rigid obstacle embedded in a homogeneous and isotropic elastic medium in two dimensions. We propose a novel boundary integral formulation and develop a highly accurate numerical method for solving the elastic obstacle scattering problem.

Given the importance of elasticity, various numerical methods have been proposed to solve the associated scattering problems in the literature. The method of boundary integral equations offers an attractive approach for solving the exterior boundary value problems such as the obstacle scattering problems. The discretization is only needed on the boundary of the domain and the radiation condition at infinity can be satisfied exactly [25], although it requires the knowledge

1991 *Mathematics Subject Classification.* 65N38, 65R20, 45L05, 45P05.

Key words and phrases. elastic wave scattering, boundary integral equation, collocation method, Helmholtz decomposition, convergence analysis.

The work of HD was supported by the NSFC grants 11801213. The work of JL was partially supported by the Funds for Creative Research Groups of NSFC (No. 11621101) and NSFC grant No. 11871427. The research of PL was supported in part by the NSF grant DMS-1912704.

of Green function for the governing equation. As is known, the Green function of the elastic wave equation is a second order tensor and the singularity is difficult to be separated in the computation of boundary integral equations, especially for the Neumann boundary condition and the three-dimensional problems. We refer to [5, 6, 23] and the references cited therein for some of the recent advances along this direction. To bypass this complexity, we introduce two scalar potential functions and use the Helmholtz decomposition to split the displacement of the elastic wave field into the compressional wave and the shear wave. The two wave components, both of which satisfy the two-dimensional Helmholtz equation [8, 19, 29], are only coupled at the boundary of the obstacle. Therefore, the boundary value problem of the Navier equation is converted equivalently into a coupled boundary value problem of the Helmholtz equations for the potentials. Such a decomposition reduces greatly the complexity for the computation of the elastic scattering problem. Similar techniques have also been successfully applied to the equations of unsteady and incompressible flow [10].

Another goal of this work is to carry out the convergence analysis of a high order numerical discretization for the boundary integral system, which requires special quadratures due to singular integral kernels [2]. The quadrature methods for the logarithmic and hypersingular integral equations were studied in [15, 18] to solve the acoustic obstacle scattering problems. Based on the trigonometric interpolation to discretize the principal part of the hypersingular operator, a fully discrete collocation method was proposed and the convergence was analyzed in [16]. In [26], the authors gave an error analysis for the collocation method used in more general singular integral operators. The bending problem of an elastic plate was discussed in [13]. A high order spectral algorithm was developed in [23] for the three-dimensional elastic obstacle scattering problem. A Nyström method with a local correction scheme was shown in [27] for the elastic obstacle scattering problem in three dimensions. We refer to [24] for a comprehensive account of the singular integral equations.

In this work, based on the Helmholtz decomposition, the exterior boundary value problem of the elastic obstacle scattering is reduced to a coupled boundary integral equation with the Cauchy type singular integral operators. Motivated by the recent works [8, 9, 19], we introduce an appropriate regularizer to the boundary integral system and split the singular integral operator into an isomorphic operator plus a compact one, which enables the convergence analysis in appropriate Sobolev spaces. The semi-discrete and full-discrete schemes are examined for the boundary integral system via the collocation method. It should be emphasized that the isomorphic operator, which consists of the modified Helmholtz single layer potential operators, is only isomorphic between the spaces we construct but not the usual L^2 space. Hence numerically it still leads to a decay spectrum with the rate of $1/N$, where N is the number of collocation points. However, we demonstrate that the proposed scheme converges exponentially fast when the boundary of the obstacle and the incident wave are analytic. Numerical experiments for both smooth and nonsmooth obstacles are provided to confirm our theoretical analysis. We point out that the proposed method is able to achieve a very high precision even for boundaries with corners by using the graded meshes [4, 7, 14]. It is also worth mentioning that our method is extremely fast since the full-discrete scheme is established via simple quadrature operators. The application of this formulation

to the elastic multi-particle scattering with the fast multipole method and inverse elastic obstacle problem have been investigated in [8, 19]. Furthermore, we extend this numerical method to the Neumann problem and the three-dimensional elastic obstacle scattering problem. This paper concerns both the theoretical analysis and numerical computation for the elastic obstacle scattering problem. It contains three contributions:

(1) prove the well-posedness of a novel boundary integral formulation by introducing a regularizer to the integral system;
(2) establish the convergence of the semi- and full-discrete schemes of the boundary integral system via the collocation method;
(3) demonstrate the superior numerical performance by presenting examples of smooth and nonsmooth obstacles, and extend this method to the Neumann boundary and three-dimensional problems.

The paper is organized as follows. In Section 2, we introduce the problem formulation. Section 3 presents the boundary integral equations, gives the decomposition of integral operators, and deduces an operator equation. Section 4 is devoted to the convergence analysis of the semi-discrete and full-discrete schemes for the boundary integral system. Numerical experiments are presented to verify the theoretical findings in Section 5. We extend this numerical method to the Neumann problem and the three-dimensional elastic obstacle scattering problem in Section 6. The paper is concluded with some general remarks and discussions on the future work in Section 7.

2. Problem formulation

Consider a two-dimensional elastically rigid obstacle, which is described as a bounded domain $D \subset \mathbb{R}^2$ with an analytic boundary Γ_D. Denote by $\nu = (\nu_1, \nu_2)^\top$ and $\tau = (\tau_1, \tau_2)^\top$ the unit normal and tangential vectors on Γ_D, respectively, where $\tau_1 = -\nu_2, \tau_2 = \nu_1$. The exterior domain $\mathbb{R}^2 \setminus \overline{D}$ is assumed to be filled with a homogeneous and isotropic elastic medium with a unit mass density.

Let the obstacle be illuminated by a time-harmonic compressional plane wave $\boldsymbol{u}^{\rm inc}(x) = d\mathrm{e}^{\mathrm{i}\kappa_{\mathtt{p}} d\cdot x}$ or shear plane wave $\boldsymbol{u}^{\rm inc}(x) = d^\perp \mathrm{e}^{\mathrm{i}\kappa_{\mathtt{s}} d\cdot x}$, where $d = (\cos\theta, \sin\theta)^\top$ is the unit propagation direction vector, $\theta \in [0, 2\pi)$ is the incident angle, $d^\perp = (-\sin\theta, \cos\theta)^\top$ is an orthonormal vector of d, and

$$\kappa_{\mathtt{p}} = \omega/(\lambda + 2\mu)^{1/2}, \quad \kappa_{\mathtt{s}} = \omega/\mu^{1/2}$$

are the compressional wavenumber and the shear wavenumber, respectively. Here $\omega > 0$ is the angular frequency and λ, μ are the Lamé constants satisfying $\mu > 0, \lambda + \mu > 0$.

The displacement of the total field $\boldsymbol{u}$ satisfies the Navier equation

$$\mu\Delta\boldsymbol{u} + (\lambda + \mu)\nabla\nabla\cdot\boldsymbol{u} + \omega^2\boldsymbol{u} = 0 \quad \text{in } \mathbb{R}^2 \setminus \overline{D}.$$

Since the obstacle is assumed to be rigid, the total field $\boldsymbol{u}$ satisfies the homogeneous Dirichlet boundary condition

$$\boldsymbol{u} = 0 \quad \text{on } \Gamma_D.$$

The total field $\boldsymbol{u}$ consists of the incident field $\boldsymbol{u}^{\rm inc}$ and the scattered field $\boldsymbol{v}$, i.e.,

$$\boldsymbol{u} = \boldsymbol{u}^{\rm inc} + \boldsymbol{v}.$$

It is easy to verify that the scattered field $\boldsymbol{v}$ satisfies the boundary value problem

$$\begin{cases} \mu\Delta\boldsymbol{v} + (\lambda+\mu)\nabla\nabla\cdot\boldsymbol{v} + \omega^2\boldsymbol{v} = 0 & \text{in } \mathbb{R}^2\setminus\overline{D}, \\ \boldsymbol{v} = -\boldsymbol{u}^{\rm inc} & \text{on } \Gamma_D. \end{cases} \tag{2.1}$$

In addition, the scattered field $\boldsymbol{v}$ is required to satisfy the Kupradze–Sommerfeld radiation condition

$$\lim_{\rho\to\infty}\rho^{\frac{1}{2}}(\partial_\rho\boldsymbol{v}_{\mathfrak{p}} - {\rm i}\kappa_{\mathfrak{p}}\boldsymbol{v}_{\mathfrak{p}}) = 0, \quad \lim_{\rho\to\infty}\rho^{\frac{1}{2}}(\partial_\rho\boldsymbol{v}_{\mathfrak{s}} - {\rm i}\kappa_{\mathfrak{s}}\boldsymbol{v}_{\mathfrak{s}}) = 0, \quad \rho = |x|,$$

where

$$\boldsymbol{v}_{\mathfrak{p}} = -\frac{1}{\kappa_{\mathfrak{p}}^2}\nabla\nabla\cdot\boldsymbol{v}, \quad \boldsymbol{v}_{\mathfrak{s}} = \frac{1}{\kappa_{\mathfrak{s}}^2}\mathbf{curl}{\rm curl}\boldsymbol{v},$$

are known as the compressional and shear wave components of $\boldsymbol{v}$, respectively. Given a vector function $\boldsymbol{v} = (v_1, v_2)^\top$ and a scalar function v, the scalar and vector curl operators are defined by

$${\rm curl}\boldsymbol{v} = \partial_{x_1}v_2 - \partial_{x_2}v_1, \quad \mathbf{curl}v = (\partial_{x_2}v, -\partial_{x_1}v)^\top.$$

For any solution $\boldsymbol{v}$ of (2.1), the Helmholtz decomposition reads

$$\boldsymbol{v} = \nabla\phi + \mathbf{curl}\psi, \tag{2.2}$$

where ϕ, ψ are two scalar functions. Combining (2.1) and (2.2) yields the Helmholtz equations

$$\Delta\phi + \kappa_{\mathfrak{p}}^2\phi = 0, \quad \Delta\psi + \kappa_{\mathfrak{s}}^2\psi = 0.$$

As usual, ϕ and ψ are required to satisfy the Sommerfeld radiation conditions

$$\lim_{\rho\to\infty}\rho^{\frac{1}{2}}(\partial_\rho\phi - {\rm i}\kappa_{\mathfrak{p}}\phi) = 0, \quad \lim_{\rho\to\infty}\rho^{\frac{1}{2}}(\partial_\rho\psi - {\rm i}\kappa_{\mathfrak{s}}\psi) = 0, \quad \rho = |x|.$$

It follows from the Helmholtz decomposition and the boundary condition on Γ_D that

$$\boldsymbol{v} = \nabla\phi + \mathbf{curl}\psi = -\boldsymbol{u}^{\rm inc}.$$

Taking the dot product of the above equation with ν and τ, respectively, we get

$$\partial_\nu\phi + \partial_\tau\psi = f_1, \quad \partial_\tau\phi - \partial_\nu\psi = f_2,$$

where

$$f_1 = -\nu\cdot\boldsymbol{u}^{\rm inc}, \quad f_2 = -\tau\cdot\boldsymbol{u}^{\rm inc}.$$

In summary, the scalar potential functions ϕ, ψ satisfy the coupled boundary value problem

$$\begin{cases} \Delta\phi + \kappa_{\mathfrak{p}}^2\phi = 0, \quad \Delta\psi + \kappa_{\mathfrak{s}}^2\psi = 0, & \text{in } \mathbb{R}^2\setminus\overline{D}, \\ \partial_\nu\phi + \partial_\tau\psi = f_1, \quad \partial_\tau\phi - \partial_\nu\psi = f_2, & \text{on } \Gamma_D, \\ \lim\limits_{\rho\to\infty}\rho^{\frac{1}{2}}(\partial_\rho\phi - {\rm i}\kappa_{\mathfrak{p}}\phi) = 0, \quad \lim\limits_{\rho\to\infty}\rho^{\frac{1}{2}}(\partial_\rho\psi - {\rm i}\kappa_{\mathfrak{s}}\psi) = 0, & \rho = |x|. \end{cases} \tag{2.3}$$

It is known that a radiating solution of (2.1) has the asymptotic behavior

$$\boldsymbol{v}(x) = \frac{{\rm e}^{{\rm i}\kappa_{\mathfrak{p}}|x|}}{\sqrt{|x|}}\boldsymbol{v}_{\mathfrak{p}}^\infty(\hat{x}) + \frac{{\rm e}^{{\rm i}\kappa_{\mathfrak{s}}|x|}}{\sqrt{|x|}}\boldsymbol{v}_{\mathfrak{s}}^\infty(\hat{x}) + \mathcal{O}\left(\frac{1}{|x|^{\frac{3}{2}}}\right), \quad |x|\to\infty \tag{2.4}$$

uniformly in all directions $\hat{x} := x/|x|$, where $\boldsymbol{v}_{\mathfrak{p}}^\infty$ and $\boldsymbol{v}_{\mathfrak{s}}^\infty$, defined on the unit circle Ω, are the compressional and shear far-field patterns of $\boldsymbol{v}$, respectively. The following result presents the relationship between the compressional (or shear) far-field pattern of $\boldsymbol{v}$ and the far-field pattern of ϕ (or ψ). The proof may be found in [8].

Lemma 2.1. *The far-field pattern* (2.4) *for the radiating solution* $\boldsymbol{v}$ *to the Navier equation satisfies*

$$\boldsymbol{v}_{\mathfrak{p}}^{\infty}(\hat{x}) = \mathrm{i}\kappa_{\mathfrak{p}}\phi_{\infty}(\hat{x})\hat{x}, \qquad \boldsymbol{v}_{\mathfrak{s}}^{\infty}(\hat{x}) = -\mathrm{i}\kappa_{\mathfrak{s}}\psi_{\infty}(\hat{x})\hat{x}^{\perp}, \tag{2.5}$$

where the complex-valued functions $\phi_{\infty}(\hat{x})$ *and* $\psi_{\infty}(\hat{x})$ *are the far-field patterns corresponding to* ϕ *and* ψ*, respectively.*

By Lemma 2.1 and the Helmholtz decomposition, it is clear to note that the elastic scattered fields $\boldsymbol{v}_{\mathfrak{p}}, \boldsymbol{v}_{\mathfrak{s}}$ and the corresponding far-field patterns $\boldsymbol{v}_{\mathfrak{p}}^{\infty}, \boldsymbol{v}_{\mathfrak{s}}^{\infty}$ can be obtained by solving the coupled boundary value problem (2.3).

3. Boundary integral equations

In this section, a novel boundary integral formulation is proposed for the coupled boundary value problem (2.3). In particular, a regularizer is constructed in order to handle the degenerated integral operators.

3.1. Coupled integral equations.

Denote the fundamental solution to the Helmholtz equation in two dimensions by

$$\Phi(x, y; \kappa) = \frac{\mathrm{i}}{4} H_0^{(1)}(\kappa|x - y|), \quad x \neq y,$$

where $H_0^{(1)}$ is the Hankel function of the first kind with order zero. Let the solution of (2.3) be given as the single-layer potentials with densities g_1, g_2:

$$\begin{cases} \phi(x) = \displaystyle\int_{\Gamma_D} \Phi(x, y; \kappa_{\mathfrak{p}}) g_1(y)\, \mathrm{d}s(y), \\ \psi(x) = \displaystyle\int_{\Gamma_D} \Phi(x, y; \kappa_{\mathfrak{s}}) g_2(y)\, \mathrm{d}s(y), \end{cases} \quad x \in \mathbb{R}^2 \setminus \Gamma_D. \tag{3.1}$$

Letting $x \in \mathbb{R}^2 \setminus \overline{D}$ approach the boundary Γ_D in (3.1), and using the jump relation of single-layer potentials and the boundary condition of (2.3), we deduce for $x \in \Gamma_D$ that

$$\begin{aligned} -\nu(x) \cdot \boldsymbol{u}^{\mathrm{inc}}(x) =& -\frac{1}{2} g_1(x) + \int_{\Gamma_D} \frac{\partial \Phi(x, y; \kappa_{\mathfrak{p}})}{\partial \nu(x)} g_1(y)\, \mathrm{d}s(y) \\ &+ \int_{\Gamma_D} \frac{\partial \Phi(x, y; \kappa_{\mathfrak{s}})}{\partial \tau(x)} g_2(y)\, \mathrm{d}s(y), \\ -\tau(x) \cdot \boldsymbol{u}^{\mathrm{inc}}(x) =& \frac{1}{2} g_2(x) + \int_{\Gamma_D} \frac{\partial \Phi(x, y; \kappa_{\mathfrak{p}})}{\partial \tau(x)} g_1(y)\, \mathrm{d}s(y) \\ &- \int_{\Gamma_D} \frac{\partial \Phi(x, y; \kappa_{\mathfrak{s}})}{\partial \nu(x)} g_2(y)\, \mathrm{d}s(y). \end{aligned} \tag{3.2}$$

The corresponding far-field patterns can be represented by

$$\begin{cases} \phi_{\infty}(\hat{x}) = \gamma_{\mathfrak{p}} \displaystyle\int_{\Gamma_D} \mathrm{e}^{-\mathrm{i}\kappa_{\mathfrak{p}}\hat{x}\cdot y} g_1(y)\, \mathrm{d}s(y), \\ \psi_{\infty}(\hat{x}) = \gamma_{\mathfrak{s}} \displaystyle\int_{\Gamma_D} \mathrm{e}^{-\mathrm{i}\kappa_{\mathfrak{s}}\hat{x}\cdot y} g_2(y)\, \mathrm{d}s(y), \end{cases} \quad \hat{x} \in \Omega, \tag{3.3}$$

where $\gamma_{\sigma} = e^{\mathrm{i}\pi/4}/\sqrt{8\kappa_{\sigma}\pi}$ for $\sigma = \mathfrak{p}$ or $\mathfrak{s}$.

We introduce the single-layer integral operator and the corresponding far-field integral operator expressed by

$$\begin{cases} (S^\sigma g)(x) = 2\displaystyle\int_{\Gamma_D} \Phi(x,y;\kappa_\sigma) g(y)\,\mathrm{d}s(y), \\ (S^\sigma_\infty g)(\hat{x}) = \gamma_\sigma \displaystyle\int_{\Gamma_D} \mathrm{e}^{-\mathrm{i}\kappa_\sigma \hat{x}\cdot y} g(y)\,\mathrm{d}s(y), \end{cases} \qquad x \in \Gamma_D,\ \hat{x} \in \Omega.$$

In addition, we introduce the normal derivative and the tangential derivative boundary integral operators

$$\begin{cases} (K^\sigma g)(x) = 2\displaystyle\int_{\Gamma_D} \frac{\partial \Phi(x,y;\kappa_\sigma)}{\partial \nu(x)} g(y)\,\mathrm{d}s(y), \\ (H^\sigma g)(x) = 2\displaystyle\int_{\Gamma_D} \frac{\partial \Phi(x,y;\kappa_\sigma)}{\partial \tau(x)} g(y)\,\mathrm{d}s(y), \end{cases} \qquad x \in \Gamma_D.$$

Note that the operators K^σ and H^σ are defined in the sense of Cauchy principal value. Based on the boundary integral operators, the coupled boundary integral equations (3.2) can be written into the operator form

$$\begin{cases} -g_1 + K^{\mathfrak{p}} g_1 + H^{\mathfrak{s}} g_2 = 2f_1, \\ g_2 + H^{\mathfrak{p}} g_1 - K^{\mathfrak{s}} g_2 = 2f_2. \end{cases} \tag{3.4}$$

Once the system (3.4) is solved for the densities g_1 and g_2, the corresponding far-field patterns of (3.3) can be represented as follows

$$\phi_\infty(\hat{x}) = (S^{\mathfrak{p}}_\infty g_1)(\hat{x}), \quad \psi_\infty(\hat{x}) = (S^{\mathfrak{s}}_\infty g_2)(\hat{x}), \qquad \hat{x} \in \Omega. \tag{3.5}$$

By [19, Theorems 4.1 and 4.8], the coupled system (3.4) is uniquely solvable if neither $\kappa_{\mathfrak{p}}$ nor $\kappa_{\mathfrak{s}}$ is the eigenvalue of the interior Dirichlet problem for the Helmholtz equation in D. Throughout, we assume that this condition is satisfied so that the system (3.4) admits a unique solution.

3.2. **Decomposition of the operators.** We assume that the boundary Γ_D is an analytic curve with the parametric form

$$\Gamma_D = \{z(t) = (z_1(t), z_2(t)) : 0 \le t < 2\pi\},$$

where $z : \mathbb{R} \to \mathbb{R}^2$ is analytic and 2π-periodic with $|z'(t)| > 0$ for all t. The parameterized integral operators are still denoted by S^σ, K^σ, H^σ, and S^σ_∞ for convenience, i.e.,

$$(S^\sigma \varphi)(t) = \frac{\mathrm{i}}{2} \int_0^{2\pi} H_0^{(1)}(\kappa_\sigma |z(t) - z(\varsigma)|) \varphi(\varsigma)\,\mathrm{d}\varsigma, \quad (K^\sigma \varphi)(t) = \int_0^{2\pi} k^\sigma(t,\varsigma)\varphi(\varsigma)\,\mathrm{d}\varsigma,$$
$$(H^\sigma \varphi)(t) = \int_0^{2\pi} h^\sigma(t,\varsigma)\varphi(\varsigma)\,\mathrm{d}\varsigma, \quad (S^\sigma_\infty \varphi)(t) = \gamma_\sigma \int_0^{2\pi} \mathrm{e}^{-\mathrm{i}\kappa_\sigma \hat{x}(t)\cdot z(\varsigma)} \varphi(\varsigma)\,\mathrm{d}\varsigma,$$

where

$$k^\sigma(t,\varsigma) = \frac{\mathrm{i}\kappa_\sigma}{2} \mathsf{n}(t) \cdot [z(\varsigma) - z(t)] \frac{H_1^{(1)}(\kappa_\sigma |z(t) - z(\varsigma)|)}{|z(t) - z(\varsigma)|},$$
$$h^\sigma(t,\varsigma) = \frac{\mathrm{i}\kappa_\sigma}{2} \mathsf{n}^\perp(t) \cdot [z(\varsigma) - z(t)] \frac{H_1^{(1)}(\kappa_\sigma |z(t) - z(\varsigma)|)}{|z(t) - z(\varsigma)|},$$

and

$$\mathsf{n}(t) \stackrel{\text{def}}{=} \tilde{\nu}(t)|z'(t)| = \big(z_2'(t), -z_1'(t)\big)^\top, \quad \tilde{\nu} = \nu \circ z,$$
$$\mathsf{n}^\perp(t) \stackrel{\text{def}}{=} \tilde{s}(t)|z'(t)| = \big(z_1'(t), z_2'(t)\big)^\top, \quad \tilde{s} = \tau \circ z.$$

Multiplying $|z'|$ on both sides of (3.4), we obtain the parametric form

$$\mathcal{A}\varphi \stackrel{\text{def}}{=} \begin{bmatrix} -I + K^{\mathfrak{p}} & H^{\mathfrak{s}} \\ H^{\mathfrak{p}} & I - K^{\mathfrak{s}} \end{bmatrix} \begin{bmatrix} \varphi_1 \\ \varphi_2 \end{bmatrix} = \begin{bmatrix} w_1 \\ w_2 \end{bmatrix}, \tag{3.6}$$

where $w_j = 2(f_j \circ z)|z'|$, $\varphi_j = (g_j \circ z)|z'|$, $j = 1, 2$, and I is the identity operator.

The kernel $k^\sigma(t, \varsigma)$ of the parameterized normal derivative integral operator can be written as

$$k^\sigma(t, \varsigma) = k_1^\sigma(t, \varsigma) \ln\Big(4 \sin^2 \frac{t - \varsigma}{2}\Big) + k_2^\sigma(t, \varsigma),$$

where

$$k_1^\sigma(t, \varsigma) = \frac{\kappa_\sigma}{2\pi} \mathsf{n}(t) \cdot \big[z(t) - z(\varsigma)\big] \frac{J_1(\kappa_\sigma |z(t) - z(\varsigma)|)}{|z(t) - z(\varsigma)|},$$
$$k_2^\sigma(t, \varsigma) = k^\sigma(t, \varsigma) - k_1^\sigma(t, \varsigma) \ln\Big(4 \sin^2 \frac{t - \varsigma}{2}\Big)$$

are analytic with diagonal entries given by

$$k_1^\sigma(t, t) = 0, \qquad k_2^\sigma(t, t) = \frac{1}{2\pi} \frac{\mathsf{n}(t) \cdot z''(t)}{|z'(t)|^2}.$$

Hence, $K^\sigma \varphi$ can be equivalently rewritten as

$$\begin{aligned}(K^\sigma \varphi)(t) &= (K_1^\sigma \varphi)(t) + (K_2^\sigma \varphi)(t) \\ &\stackrel{\text{def}}{=} \int_0^{2\pi} \ln\Big(4 \sin^2 \frac{t - \varsigma}{2}\Big) k_1^\sigma(t, \varsigma) \varphi(\varsigma)\, \mathrm{d}\varsigma + \int_0^{2\pi} k_2^\sigma(t, \varsigma) \varphi(\varsigma)\, \mathrm{d}\varsigma.\end{aligned}$$

Following [8], we split the kernel $h^\sigma(t, \varsigma)$ of the parameterized tangential derivative integral operator into

$$h^\sigma(t, \varsigma) = h_1(t, \varsigma) \cot \frac{\varsigma - t}{2} + h_2^\sigma(t, \varsigma) \ln\Big(4 \sin^2 \frac{t - \varsigma}{2}\Big) + h_3^\sigma(t, \varsigma), \tag{3.7}$$

where

$$h_1(t, \varsigma) = \frac{1}{\pi} n^\perp(t) \cdot \big[z(\varsigma) - z(t)\big] \frac{\tan \frac{\varsigma - t}{2}}{|z(t) - z(\varsigma)|^2},$$
$$h_2^\sigma(t, \varsigma) = \frac{\kappa_\sigma}{2\pi} n^\perp(t) \cdot \big[z(t) - z(\varsigma)\big] \frac{J_1(\kappa_\sigma |z(t) - z(\varsigma)|)}{|z(t) - z(\varsigma)|},$$
$$h_3^\sigma(t, \varsigma) = h^\sigma(t, \varsigma) - h_1^\sigma(t, \varsigma) \cot \frac{\varsigma - t}{2} - h_2^\sigma(t, \varsigma) \ln\Big(4 \sin^2 \frac{t - \varsigma}{2}\Big)$$

are analytic with diagonal entries given by

$$h_1(t, t) = \frac{1}{2\pi}, \quad h_2^\sigma(t, t) = 0, \quad h_3^\sigma(t, t) = 0.$$

In order to show the convergence, based on (3.7), we split the singular integral operator H^σ into

$$H^\sigma = H_1 + E^\sigma H_2 + \widetilde{H}_1 + \widetilde{H}_2^\sigma + \widetilde{H}_3^\sigma, \tag{3.8}$$

where $E^\sigma\psi = \kappa_\sigma^2|z'|^2\psi$, and

$$(H_1\psi)(t) = \frac{1}{2\pi}\int_0^{2\pi} \cot\frac{\varsigma - t}{2}\psi(\varsigma)\,\mathrm{d}\varsigma + \frac{\mathrm{i}}{2\pi}\int_0^{2\pi}\psi(\varsigma)\,\mathrm{d}\varsigma,$$
$$(H_2\psi)(t) = \frac{1}{4\pi}\int_0^{2\pi} \ln\Big(4\sin^2\frac{t-\varsigma}{2}\Big)\sin(t-\varsigma)\psi(\varsigma)\,\mathrm{d}\varsigma + \frac{\mathrm{i}}{2\pi}\int_0^{2\pi}\psi(\varsigma)\,\mathrm{d}\varsigma,$$
$$(\widetilde{H}_1\psi)(t) = \int_0^{2\pi}\widetilde{h}_1(t,\varsigma)\psi(\varsigma)\,\mathrm{d}\varsigma, \quad (\widetilde{H}_2^\sigma\psi)(t) = \int_0^{2\pi}\ln\Big(4\sin^2\frac{t-\varsigma}{2}\Big)\widetilde{h}_2^\sigma(t,\varsigma)\psi(\varsigma)\,\mathrm{d}\varsigma,$$
$$(\widetilde{H}_3^\sigma\psi)(t) = \int_0^{2\pi}\widetilde{h}_3^\sigma(t,\varsigma)\psi(\varsigma)\,\mathrm{d}\varsigma.$$

Here, the functions

$$\widetilde{h}_1(t,\varsigma) = \cot\frac{\varsigma-t}{2}\big(h_1(t,\varsigma) - \frac{1}{2\pi}\big),$$
$$\widetilde{h}_2^\sigma(t,\varsigma) = h_2^\sigma(t,\varsigma) - \kappa_\sigma^2/(4\pi)|z'(t)|^2\sin(t-\varsigma),$$
$$\widetilde{h}_3^\sigma(t,\varsigma) = h_3^\sigma(t,\varsigma) - \mathrm{i}\frac{\kappa_\sigma^2|z'(t)|^2+1}{2\pi}$$

are analytic with diagonal entries $\widetilde{h}_1(t,t) = \widetilde{h}_2^\sigma(t,t) = 0$. We refer to the proof of Theorem 3.3 for the analyticity of $\widetilde{h}_1$.

3.3. **Operator equations.** We reformulate the parametrized integral equations (3.6) into a single operator form

$$\mathcal{A}\varphi = (\mathcal{H} + \mathcal{B})\varphi = w, \tag{3.9}$$

where $\varphi = (\varphi_1, \varphi_2)^\top$, $w = (w_1, w_2)^\top$ and

$$\mathcal{H} = \begin{bmatrix} -I & H_1 \\ H_1 & I \end{bmatrix} + \begin{bmatrix} 0 & E^{\mathfrak{s}}H_2 \\ E^{\mathfrak{p}}H_2 & 0 \end{bmatrix} \overset{\text{def}}{=} \mathcal{H}_1 + \mathcal{H}_2,$$
$$\mathcal{B} = \mathcal{B}_1 + \mathcal{B}_2 + \mathcal{B}_3 \overset{\text{def}}{=} \begin{bmatrix} K_1^{\mathfrak{p}} & \widetilde{H}_2^{\mathfrak{s}} \\ \widetilde{H}_2^{\mathfrak{p}} & -K_1^{\mathfrak{s}} \end{bmatrix} + \begin{bmatrix} K_2^{\mathfrak{p}} & \widetilde{H}_3^{\mathfrak{s}} \\ \widetilde{H}_3^{\mathfrak{p}} & -K_2^{\mathfrak{s}} \end{bmatrix} + \begin{bmatrix} 0 & \widetilde{H}_1 \\ \widetilde{H}_1 & 0 \end{bmatrix}.$$

More specifically, we have

$$(\mathcal{B}_1\varphi)(t) = \int_0^{2\pi}\ln\Big(4\sin^2\frac{t-\varsigma}{2}\Big)\begin{bmatrix} k_1^{\mathfrak{p}}(t,\varsigma) & \widetilde{h}_2^{\mathfrak{s}}(t,\varsigma) \\ \widetilde{h}_2^{\mathfrak{p}}(t,\varsigma) & -k_1^{\mathfrak{s}}(t,\varsigma)\end{bmatrix}\begin{bmatrix}\varphi_1(\varsigma)\\ \varphi_2(\varsigma)\end{bmatrix}\mathrm{d}\varsigma,$$
$$(\mathcal{B}_2\varphi + \mathcal{B}_3\varphi)(t) = \int_0^{2\pi}\begin{bmatrix} k_2^{\mathfrak{p}}(t,\varsigma) & \widetilde{h}_3^{\mathfrak{s}}(t,\varsigma) + \widetilde{h}_1(t,\varsigma) \\ \widetilde{h}_3^{\mathfrak{p}}(t,\varsigma) + \widetilde{h}_1(t,\varsigma) & -k_2^{\mathfrak{s}}(t,\varsigma)\end{bmatrix}\begin{bmatrix}\varphi_1(\varsigma)\\ \varphi_2(\varsigma)\end{bmatrix}\mathrm{d}\varsigma.$$

Let $H^p[0,2\pi], p \geq 0$ denote the space of 2π-periodic functions $u : \mathbb{R} \to \mathbb{C}$ equipped with the norm

$$\|u\|_p^2 := \sum_{m=-\infty}^{\infty}(1+m^2)^p|\hat{u}_m|^2 < \infty,$$

where

$$\hat{u}_m = \frac{1}{2\pi}\int_0^{2\pi}u(t)e^{-\mathrm{i}mt}\,\mathrm{d}t, \qquad m = 0, \pm1, \pm2, \cdots$$

are the Fourier coefficients of u. Define Sobolev spaces

$$H^p[0,2\pi]^2 = \left\{ w = (w_1, w_2)^\top ; w_1(t) \in H^p[0,2\pi], w_2(t) \in H^p[0,2\pi] \right\},$$
$$H^p_*[0,2\pi]^2 = \left\{ w = (w_1, w_2)^\top ; w(t) \in H^p[0,2\pi]^2, (\mathcal{H}_1 w)(t) \in H^{p+2}[0,2\pi]^2 \right\},$$

which are equipped with the norms

$$\begin{aligned} \|w\|_p &= \|w_1\|_p + \|w_2\|_p, \\ \|w\|_{p,*} &= \|w_1\|_p + \|w_2\|_p + \|H_1 w_2 - w_1\|_{p+2} + \|H_1 w_1 + w_2\|_{p+2}. \end{aligned} \tag{3.10}$$

It is easy to see the embedding relation $H^{p+2}[0,2\pi]^2 \hookrightarrow H^p_*[0,2\pi]^2 \hookrightarrow H^p[0,2\pi]^2$, since $H_1 : H^p[0,2\pi] \to H^p[0,2\pi]$ is bounded (cf. Theorem 3.2).

It is difficult to analyze directly the operator equation (3.9) since the leading term $\mathcal{H}_1$ is degenerated [19]. To overcome this difficulty, we introduce a regularizer via multiplying both sides of (3.9) by $\mathcal{A}$. Now, we consider the regularized equation

$$\mathcal{A}^2 \varphi = (\mathcal{H}^2 + \mathcal{H}\mathcal{B} + \mathcal{B}\mathcal{H} + \mathcal{B}^2)\varphi = \mathcal{A} w, \tag{3.11}$$

which is equivalent to (3.9) since $\mathcal{A}$ is invertible.

Theorem 3.1. *The operator $E^\sigma : H^p[0,2\pi] \to H^p[0,2\pi]$ is bounded.*

Proof. Recalling $E^\sigma \varphi = \kappa_\sigma^2 a(t)\varphi$ for $\sigma = \mathfrak{p}, \mathfrak{s}$, where $a(t) = |z'(t)|^2$ and is analytic, we may assume

$$a(t) = \sum_{m=-\infty}^{\infty} \hat{a}_m \mathrm{e}^{\mathrm{i}mt},$$

where $\hat{a}_m$ are the Fourier coefficients of a. The analyticity of a implies that

$$\sup_{m\in\mathbb{Z}} |m|^l |\hat{a}_m| < \infty \quad \forall\, l \geq 0,$$

which, together with [17, Corollary 8.8], gives

$$\|E^\sigma \varphi\|_p \leq c_1 \sum_{m=-\infty}^{\infty} |\hat{a}_m| |m|^k \|\varphi\|_p \leq c_1 \sum_{m=-\infty}^{\infty} |\hat{a}_m| \frac{(1+m^2)^{k/2+1}}{1+m^2} \|\varphi\|_p \leq c_2 \|\varphi\|_p,$$

where the first inequality holds for all $k \geq p$. □

Theorem 3.2. *The operator $\mathcal{H} : H^p[0,2\pi]^2 \to H^p_*[0,2\pi]^2$ is bounded.*

Proof. For the trigonometric basis functions $f_m(t) := \mathrm{e}^{\mathrm{i}mt}, \forall m \in \mathbb{Z}$, noting

$$H_1 f_m = \zeta_m f_m, \qquad \zeta_m = \begin{cases} \mathrm{i}\,\mathrm{sign}(m), & m \neq 0, \\ \mathrm{i}, & m = 0, \end{cases}$$
$$H_2 f_m = \xi_m f_m, \qquad \xi_m = \begin{cases} \frac{\mathrm{i}}{4}\left(\frac{1}{|m-1|} - \frac{1}{|m+1|}\right), & m = \pm 2, \pm 3, \cdots, \\ -\frac{\mathrm{i}}{8}\mathrm{sign}(m), & m = \pm 1, \\ \mathrm{i}, & m = 0, \end{cases}$$

we observe that the integral operators $H_1 : H^p[0,2\pi] \to H^p[0,2\pi]$ and $H_2 : H^p[0,2\pi] \to H^{p+2}[0,2\pi]$ are bounded for arbitrary $p \geq 0$. Then, $\forall \varphi = (\varphi_1, \varphi_2)^\top \in$

$H^p[0,2\pi]^2$, using $H_1H_1+I=0$ and (3.10), we have

$$\begin{aligned}\|\mathcal{H}_1\varphi\|_{p,*} &= \|(H_1\varphi_2-\varphi_1, H_1\varphi_1+\varphi_2)^\top\|_{p,*}\\ &= \|H_1\varphi_2-\varphi_1\|_p + \|H_1(H_1\varphi_1+\varphi_2)-(H_1\varphi_2-\varphi_1)\|_{p+2}\\ &\quad + \|H_1\varphi_1+\varphi_2\|_p + \|H_1(H_1\varphi_2-\varphi_1)+H_1\varphi_1+\varphi_2\|_{p+2}\\ &= \|H_1\varphi_2-\varphi_1\|_p + \|H_1\varphi_1+\varphi_2\|_p \le C_1\|\varphi\|_p.\end{aligned}$$

By Theorem 3.1, we get

$$\begin{aligned}\|\mathcal{H}_2\varphi\|_{p,*} &\le C_2\|\mathcal{H}_2\varphi\|_{p+2} = C_2\|E^{\mathfrak{p}}H_2\varphi_1\|_{p+2} + C_2\|E^{\mathfrak{s}}H_2\varphi_2\|_{p+2}\\ &\le C_3(\|\varphi_1\|_p+\|\varphi_2\|_p) = C_3\|\varphi\|_p,\end{aligned}$$

where C_1, C_2, C_3 are positive constants. Combining the above estimates shows that $\mathcal{H}=\mathcal{H}_1+\mathcal{H}_2 : H^p[0,2\pi]^2 \to H^p_*[0,2\pi]^2$ is bounded. □

Theorem 3.3. *The operator $\mathcal{B} : H^p[0,2\pi]^2 \to H^{p+2}[0,2\pi]^2$ is compact.*

Proof. First we show that $\mathcal{B}_1$ and $\mathcal{B}_2$ are compact. Noting

$$k_1^\sigma(t,t)=\partial_t k_1^\sigma(t,t)=0, \qquad \widetilde{h}_2^\sigma(t,t)=\partial_t\widetilde{h}_2^\sigma(t,t)=0, \quad \sigma=\mathfrak{p},\mathfrak{s}, \tag{3.12}$$

and using [17, Theorems 12.15, 13.20], we get that $K_1^\sigma, H_2^\sigma : H^p[0,2\pi] \to H^{p+3}[0,2\pi]$ are bounded for arbitrary $p\ge 0$. Thus $\mathcal{B}_1 : H^p[0,2\pi]^2 \to H^{p+3}[0,2\pi]^2$ is bounded and consequently is compact from $H^p[0,2\pi]^2$ into $H^{p+2}[0,2\pi]^2$. Since the kernel functions k_2 and $\widetilde{h}_3$ are analytic, it follows from [12, Theorem A.45] and [17, Theorem 8.13] that the operators $K_2^\sigma, \widetilde{H}_3^\sigma : H^p[0,2\pi] \to H^{p+r}[0,2\pi]$ are bounded for all integers $r\ge 0$ and arbitrary $p\ge 0$. Then the operator $\mathcal{B}_2 : H^p[0,2\pi]^2 \to H^{p+r}[0,2\pi]^2$ is bounded for all integers $r\ge 0$ and arbitrary $p\ge 0$. In particular, the operator $\mathcal{B}_2 : H^p[0,2\pi]^2 \to H^{p+3}[0,2\pi]^2, \forall p\ge 0$ is bounded and consequently is compact from $H^p[0,2\pi]^2$ into $H^{p+2}[0,2\pi]^2$.

Next is to show the compactness of $\mathcal{B}_3$. It suffices to show that $\widetilde{H}_1$ has an analytic kernel $\widetilde{h}_1$. In fact, for ς sufficiently close to t, by using the Taylor expansions

$$\begin{aligned}\tan\frac{\varsigma-t}{2} &= \sum_{k=1}^\infty a_k\Big(\frac{\varsigma-t}{2}\Big)^{2k-1},\ a_k>0,\ a_1=1,\\ n^\perp(t)\cdot\big[z(\varsigma)-z(t)\big] &= |z'(t)|^2(\varsigma-t)\Big(1+\sum_{k=1}^\infty b_k(t)(\varsigma-t)^k\Big),\\ |z(t)-z(\varsigma)|^2 &= |z'(t)|^2(\varsigma-t)^2\Big(1+\sum_{k=1}^\infty d_k(t)(\varsigma-t)^k\Big)\\ &\stackrel{\rm def}{=} |z'(t)|^2(\varsigma-t)^2(1+\Theta),\end{aligned}$$

we have

$$\begin{aligned}h_1(t,\varsigma) &= \frac{1}{\pi}n^\perp(t)\cdot\big[z(\varsigma)-z(t)\big]\frac{\tan\frac{\varsigma-t}{2}}{|z(t)-z(\varsigma)|^2}\\ &= \frac{1}{2\pi}\Big(1+\sum_{k=1}^\infty b_k(t)(\varsigma-t)^k\Big)(1-\Theta+\Theta^2-\Theta^3+\cdots)\sum_{k=1}^\infty a_k\Big(\frac{\varsigma-t}{2}\Big)^{2k-2}\\ &= \frac{1}{2\pi}+\sum_{k=1}^\infty c_k(t)(\varsigma-t)^k.\end{aligned}$$

Moreover, it can be easily verified that

$$c_1(t) = \frac{b_1(t) - d_1(t)}{2\pi} = -\frac{z_1'(t)z_1''(t) + z_2'(t)z_2''(t)}{4\pi|z'(t)|^2} \not\equiv 0.$$

Using the Taylor expansions for sine and cosine functions, we deduce that the kernel function has the expansion

$$\widetilde{h}_1(t,\varsigma) = \cot\frac{\varsigma - t}{2}\sum_{k=1}^{\infty} c_k(t)(\varsigma - t)^k = \sum_{k=1}^{\infty} e_k(t)(\varsigma - t)^k, \quad e_1(t) = 2c_1(t),$$

which implies that $\widetilde{h}_1$ is analytic and completes the proof. □

By [17, Theorem 8.24], the operator $S_0 : H^p[0,2\pi] \to H^{p+1}[0,2\pi]$, defined by

$$(S_0\psi)(t) = \int_0^{2\pi} \ln\Big(4\sin^2\frac{t-\varsigma}{2}\Big)\psi(\varsigma)\,\mathrm{d}\varsigma + \sqrt{2}\mathrm{i}\int_0^{2\pi}\psi(\varsigma)\,\mathrm{d}\varsigma \stackrel{\text{def}}{=} (\widetilde{S}_0\psi)(t) + M_0,$$

is bounded and has a bounded inverse for all $p \geq 0$. We denote the operators $\mathcal{S}_0$ and $\mathcal{E}$ by

$$\mathcal{S}_0 = \begin{bmatrix} S_0 & 0 \\ 0 & S_0 \end{bmatrix}, \quad \mathcal{E} = \frac{1}{8\pi^2}\begin{bmatrix} E^{\mathfrak{p}} + E^{\mathfrak{s}} & 0 \\ 0 & E^{\mathfrak{p}} + E^{\mathfrak{s}} \end{bmatrix}.$$

Clearly, $\mathcal{S}_0\mathcal{S}_0$ is an isomorphism from $H^p[0,2\pi]^2$ to $H^{p+2}[0,2\pi]^2$ and $\mathcal{E}$ is an isomorphism from $H^p[0,2\pi]^2$ to $H^p[0,2\pi]^2$ since $a(t)$ is analytic and $a(t) \neq 0$.

Theorem 3.4. *For any function $\varphi \in H^p[0,2\pi]^2$, the operator $\mathcal{H}^2 : H^p[0,2\pi]^2 \to H^{p+2}[0,2\pi]^2$ can be expressed as*

$$\mathcal{H}^2\varphi = (\mathcal{E}\mathcal{S}_0\mathcal{S}_0 + \mathcal{J})\varphi,$$

where $\mathcal{J}$ is a compact operator from $H^p[0,2\pi]^2$ into $H^{p+2}[0,2\pi]^2$.

Proof. It follows from a straightforward calculation that

$$\begin{aligned}\mathcal{H}^2 &= \begin{bmatrix} -I & H_1 + E^{\mathfrak{s}}H_2 \\ H_1 + E^{\mathfrak{p}}H_2 & I \end{bmatrix}\begin{bmatrix} -I & H_1 + E^{\mathfrak{s}}H_2 \\ H_1 + E^{\mathfrak{p}}H_2 & I \end{bmatrix} \\ &= \begin{bmatrix} H_1E^{\mathfrak{p}}H_2 + E^{\mathfrak{s}}H_2H_1 & 0 \\ 0 & H_1E^{\mathfrak{s}}H_2 + E^{\mathfrak{p}}H_2H_1 \end{bmatrix} + \mathcal{J}_1,\end{aligned}$$

where

$$\begin{aligned}\mathcal{J}_1 &= \begin{bmatrix} E^{\mathfrak{s}}J_1^{\mathfrak{p}}H_2 & 0 \\ 0 & E^{\mathfrak{p}}J_1^{\mathfrak{s}}H_2 \end{bmatrix} + \begin{bmatrix} E^{\mathfrak{s}}E^{\mathfrak{p}}H_2H_2 & 0 \\ 0 & E^{\mathfrak{p}}E^{\mathfrak{s}}H_2H_2 \end{bmatrix}, \\ J_1^{\sigma}\psi &= H_2E^{\sigma}\psi - E^{\sigma}H_2\psi \\ &= \frac{\kappa_\sigma^2}{4\pi}\int_0^{2\pi}\ln\Big(4\sin^2\frac{t-\varsigma}{2}\Big)\sin(t-\varsigma)\Big(|z'(\varsigma)|^2 - |z'(t)|^2\Big)\psi(\varsigma)\,\mathrm{d}\varsigma \\ &\quad + \frac{\mathrm{i}\kappa_\sigma^2}{2\pi}\int_0^{2\pi}\Big(|z'(\varsigma)|^2 - |z'(t)|^2\Big)\psi(\varsigma)\,\mathrm{d}\varsigma,\end{aligned}$$

and $\mathcal{J}_1$ is bounded from $H^p[0,2\pi]^2$ to $H^{p+4}[0,2\pi]^2$ and consequently is compact from $H^p[0,2\pi]^2$ into $H^{p+2}[0,2\pi]^2$.

For the first term of $\mathcal{H}^2$, we rewrite the first diagonal element by

$$H_1E^{\mathfrak{p}}H_2 + E^{\mathfrak{s}}H_2H_1 = E^{\mathfrak{p}}H_1H_2 + E^{\mathfrak{s}}H_2H_1 + J_2^{\mathfrak{p}},$$

where $J_2^{\mathfrak{p}}\psi = H_1 E^{\mathfrak{p}} H_2\psi - E^{\mathfrak{p}} H_1 H_2\psi = \widetilde{J}_2^{\mathfrak{p}} H_2\psi$ and

$$(\widetilde{J}_2^{\mathfrak{p}}\psi)(t) = \frac{\kappa_{\mathfrak{p}}^2}{2\pi}\int_0^{2\pi} \cot\frac{t-\varsigma}{2}\Big(|z'(\varsigma)|^2 - |z'(t)|^2\Big)\psi(\varsigma)\,\mathrm{d}\varsigma + \frac{\mathrm{i}\kappa_{\mathfrak{p}}^2}{2\pi}\int_0^{2\pi}\Big(|z'(\varsigma)|^2 - |z'(t)|^2\Big)\psi(\varsigma)\,\mathrm{d}\varsigma.$$

The operator $J_2^{\mathfrak{p}}$ is compact from $H^p[0,2\pi]^2$ into $H^{p+2}[0,2\pi]^2$, since the operator $\widetilde{J}_2^{\mathfrak{p}}$ has an analytic kernel and H_2 is bounded. In addition, for $\psi \in H^p[0,2\pi]$, we have

$$\begin{aligned}(H_1H_2\psi)(t) =& \frac{1}{2\pi}\int_0^{2\pi}\cot\frac{t-\varsigma}{2}(H_2\psi)(\varsigma)\,\mathrm{d}\varsigma + \frac{\mathrm{i}}{2\pi}\int_0^{2\pi}(H_2\psi)(\varsigma)\,\mathrm{d}\varsigma\\ =& \frac{1}{2\pi}\int_0^{2\pi}\ln\Big(4\sin^2\frac{t-\varsigma}{2}\Big)\frac{\mathrm{d}}{\mathrm{d}\varsigma}(H_2\psi)(\varsigma)\,\mathrm{d}\varsigma + \frac{\mathrm{i}}{2\pi}\xi_0\hat{\psi}_0 2\pi\\ =& \frac{1}{8\pi^2}\int_0^{2\pi}\ln\Big(4\sin^2\frac{t-\varsigma}{2}\Big)\int_0^{2\pi}\ln\Big(4\sin^2\frac{\varsigma-s}{2}\Big)\psi(s)\,\mathrm{d}s\,\mathrm{d}\varsigma\\ & - \hat{\psi}_0 + \frac{1}{8\pi^2}(J_3\psi + J_4\psi)(t)\\ =& \frac{1}{8\pi^2}(S_0S_0\psi)(t) + \frac{1}{8\pi^2}(J_3\psi)(t) + \frac{1}{8\pi^2}(J_4\psi)(t),\end{aligned}$$

where

$$\begin{aligned}(J_3\psi)(t) &= \int_0^{2\pi}\ln\Big(4\sin^2\frac{t-\varsigma}{2}\Big)\int_0^{2\pi}\cot\frac{\varsigma-s}{2}\sin(\varsigma-s)\psi(s)\,\mathrm{d}s \stackrel{\mathrm{def}}{=} (\widetilde{S}_0\widetilde{J}_3\psi)(t),\\ (J_4\psi)(t) &= \int_0^{2\pi}\ln\Big(4\sin^2\frac{t-\varsigma}{2}\Big)\int_0^{2\pi}\ln\Big(4\sin^2\frac{\varsigma-s}{2}\Big)(\cos(\varsigma-s)-1)\psi(s)\,\mathrm{d}s\\ &\stackrel{\mathrm{def}}{=} (\widetilde{S}_0\widetilde{J}_4\psi)(t),\end{aligned}$$

are compact from $H^p[0,2\pi]^2$ into $H^{p+2}[0,2\pi]^2$, since the operator $\widetilde{J}_3$ has an analytic kernel, and the operators $\widetilde{S}_0 : H^p[0,2\pi]^2 \to H^{p+1}[0,2\pi]^2$ and $J_4 : H^p[0,2\pi]^2 \to H^{p+3}[0,2\pi]^2$ are bounded. Clearly it also holds that $H_2H_1 = H_1H_2$.

Similarly, we can analyze the second diagonal element as the first one. Therefore, we obtain the assertion of the theorem by defining the operator

$$\mathcal{J} = \mathcal{J}_1 + \mathcal{J}_2 + \mathcal{J}_3 + \mathcal{J}_4,$$

where

$$\mathcal{J}_2 = \begin{bmatrix} J_2^{\mathfrak{p}} & 0\\ 0 & J_2^{\mathfrak{s}}\end{bmatrix},\quad \mathcal{J}_3 = \frac{\kappa_{\mathfrak{p}}^2+\kappa_{\mathfrak{s}}^2}{8\pi^2}|z'|^2\begin{bmatrix} J_3 & 0\\ 0 & J_3\end{bmatrix},$$
$$\mathcal{J}_4 = \frac{\kappa_{\mathfrak{p}}^2+\kappa_{\mathfrak{s}}^2}{8\pi^2}|z'|^2\begin{bmatrix} J_4 & 0\\ 0 & J_4\end{bmatrix}.$$

□

4. Collocation method

Consider the following equivalent formulation of the operator equation (3.11):

$$\mathcal{S}_0\mathcal{S}_0\varphi + \mathcal{E}^{-1}(\mathcal{J}+\mathcal{K})\varphi = \mathcal{E}^{-1}\mathcal{A}w, \tag{4.1}$$

where $\mathcal{K} \stackrel{\text{def}}{=} \mathcal{H}\mathcal{B}+\mathcal{B}\mathcal{H}+\mathcal{B}^2$ is a compact operator from $H^p[0,2\pi]^2$ into $H^{p+2}[0,2\pi]^2$ by Theorems 3.2 and 3.3. In this section, we examine the convergence of the semi- and full-discretization of (4.1) by using the collocation method.

4.1. **Semi-discretization.** Let X_n be the space of trigonometric polynomials of degree less than or equal to n of the form

$$\varphi(t) = \sum_{m=0}^{n} \alpha_m \cos mt + \sum_{m=1}^{n-1} \beta_m \sin mt. \tag{4.2}$$

Denote by $P_n : H^p[0,2\pi] \to X_n$ the interpolation operator, which maps 2π-periodic scalar function g into a unique trigonometric polynomial $P_n g$ at the equidistant interpolation points $\varsigma_j^{(n)} := \pi j/n$, $j = 0, \cdots, 2n-1$, i.e., $(P_n g)(\varsigma_j^{(n)}) = g(\varsigma_j^{(n)})$. Then, P_n is a bounded linear operator.

Let $X_n^2 = \{\varphi = (\varphi_1, \varphi_2)^\top : \varphi_1 \in X_n, \varphi_2 \in X_n\}$ and define the interpolation operator $\mathcal{P}_n : H^p[0,2\pi]^2 \to X_n^2$ by

$$\mathcal{P}_n g = (P_n g_1, P_n g_2)^\top, \quad \forall\, g = (g_1, g_2) \in H^p[0,2\pi]^2.$$

Clearly, X_n^2 is unisolvent with respect to the points $\{\varsigma_j^{(n)}\}_{j=0}^{2n-1}$. Moreover, we have from [17, Theorem 11.8] that

$$\|\mathcal{P}_n g - g\|_q \le \frac{C}{n^{p-q}} \|g\|_p, \qquad 0 \le q \le p, \quad \frac{1}{2} < p \tag{4.3}$$

for all $g \in H^p[0,2\pi]^2$ and some constant C depending on p and q.

Now we approximate the solution $\varphi = (\varphi_1, \varphi_2)^\top$ by a trigonometric polynomial $\varphi^n = (\varphi_1^n, \varphi_2^n)^\top \in X_n^2$, which is required to satisfy the projected equation

$$\mathcal{S}_0\mathcal{S}_0\varphi^n + \mathcal{P}_n[\mathcal{E}^{-1}(\mathcal{J}+\mathcal{K})]\varphi^n = \mathcal{P}_n(\mathcal{E}^{-1}\mathcal{A})w, \tag{4.4}$$

where φ^n satisfies $\mathcal{P}_n(\mathcal{S}_0\mathcal{S}_0)\varphi^n = \mathcal{S}_0\mathcal{S}_0\varphi^n$.

Theorem 4.1. *For sufficiently large n, the approximate equation* (4.4) *is uniquely solvable and the solution satisfies the error estimate*

$$\|\varphi^n - \varphi\|_p \le L\|\mathcal{P}_n\mathcal{S}_0\mathcal{S}_0\varphi - \mathcal{S}_0\mathcal{S}_0\varphi\|_{p+2},$$

where L is a positive constant depending on $\mathcal{E}^{-1}\mathcal{J}$, $\mathcal{E}^{-1}\mathcal{K}$ and $\mathcal{S}_0\mathcal{S}_0$.

Proof. By the proofs of Theorems 3.3 and 3.4, we know that the operators $\mathcal{J}, \mathcal{K} : H^p[0,2\pi]^2 \to H^{p+3}[0,2\pi]^2, \forall p \ge 0$ are bounded. With the aid of (4.3), we deduce that

$$\|\mathcal{P}_n[\mathcal{E}^{-1}(\mathcal{J}+\mathcal{K})]\varphi - \mathcal{E}^{-1}(\mathcal{J}+\mathcal{K})\varphi\|_{p+2} \le \frac{c_1}{n}\|\mathcal{E}^{-1}(\mathcal{J}+\mathcal{K})\varphi\|_{p+3} \le \frac{c_2}{n}\|\varphi\|_p$$

for all $p \ge 0$ and some constants c_1 and c_2, which implies

$$\|\mathcal{P}_n[\mathcal{E}^{-1}(\mathcal{J}+\mathcal{K})] - \mathcal{E}^{-1}(\mathcal{J}+\mathcal{K})\|_{p+2} \to 0 \quad \text{as} \quad n \to \infty.$$

The proof is completed by noting [17, Theorem 13.12]. □

The above theorem implies that the semi-discrete collocation method given by (4.4) converges in $H^p[0,2\pi]^2$ for each $p \ge 0$.

4.2. **Full-discretization.** Denote the Lagrange basis by

$$\mathfrak{L}_j(t)=\frac{1}{2n}\left\{1+2\sum_{k=1}^{n-1}\cos k(t-\varsigma_j^{(n)})+\cos n(t-\varsigma_j^{(n)})\right\},\quad j=0,1,\cdots,2n-1.$$

Instead of (4.4), we find an approximate solution $\widetilde{\varphi}^n\in X_n^2$ given by

$$\widetilde{\varphi}^n(t)=\big(\widetilde{\varphi}_1^n(t),\widetilde{\varphi}_2^n(t)\big)^\top=\Big(\sum_{j=0}^{2n-1}\widetilde{\varphi}_1^n(\varsigma_j^{(n)})\mathfrak{L}_j(t),\sum_{j=0}^{2n-1}\widetilde{\varphi}_2^n(\varsigma_j^{(n)})\mathfrak{L}_j(t)\Big)^\top,$$

which is required to satisfy

$$\mathcal{S}_{0,n}\mathcal{S}_{0,n}\widetilde{\varphi}^n+\mathcal{P}_n[\mathcal{E}_n^{-1}(\mathcal{J}_n+\mathcal{K}_n)]\widetilde{\varphi}^n=\mathcal{P}_n(\mathcal{E}_n^{-1}\mathcal{A}_n)w. \tag{4.5}$$

Here $\mathcal{A}_n=\mathcal{H}_n+\mathcal{B}_n=\sum_{j=1}^{2}\mathcal{H}_{j,n}+\sum_{j=1}^{3}\mathcal{B}_{j,n}$, $\mathcal{J}_n=\sum_{j=1}^{4}\mathcal{J}_{j,n}$, $\mathcal{K}_n=\mathcal{H}_n\mathcal{B}_n+\mathcal{B}_n\mathcal{H}_n+\mathcal{B}_n\mathcal{B}_n$, and the quadrature operators are described by $\mathcal{S}_{0,n}=\mathcal{S}_0\mathcal{P}_n$, $\mathcal{H}_{1,n}=\mathcal{H}_1\mathcal{P}_n$, $\mathcal{H}_{2,n}=\mathcal{H}_2\mathcal{P}_n$,

$$(\mathcal{B}_{1,n}\chi)(t)=\int_0^{2\pi}\ln\Big(4\sin^2\frac{t-\varsigma}{2}\Big)\mathcal{P}_n\left\{\begin{bmatrix}k_1^{\mathfrak{p}}(t,\cdot)&\widetilde{h}_2^{\mathfrak{s}}(t,\cdot)\\ \widetilde{h}_2^{\mathfrak{p}}(t,\cdot)&-k_1^{\mathfrak{s}}(t,\cdot;)\end{bmatrix}\chi\right\}(\varsigma)\,\mathrm{d}\varsigma,$$

$$(\mathcal{B}_{2,n}\chi+\mathcal{B}_{3,n}\chi)(t)=\int_0^{2\pi}\mathcal{P}_n\left\{\begin{bmatrix}k_2^{\mathfrak{p}}(t,\cdot)&\widetilde{h}_3^{\mathfrak{s}}(t,\cdot)+\widetilde{h}_1(t,\cdot)\\ \widetilde{h}_3^{\mathfrak{p}}(t,\cdot)+\widetilde{h}_1(t,\cdot)&-k_2^{\mathfrak{s}}(t,\cdot)\end{bmatrix}\chi\right\}(\varsigma)\,\mathrm{d}\varsigma.$$

Define $E_n^\sigma\psi=\kappa_\sigma^2|z'|^2\psi=E^\sigma\psi$, $H_{2,n}=H_2P_n$, $\widetilde{S}_{0,n}=\widetilde{S}_0P_n$,

$$\mathcal{E}_n=\frac{1}{8\pi^2}\begin{bmatrix}E_n^{\mathfrak{p}}+E_n^{\mathfrak{s}}&0\\0&E_n^{\mathfrak{p}}+E_n^{\mathfrak{s}}\end{bmatrix},$$

$$\mathcal{J}_{1,n}=\begin{bmatrix}E_n^{\mathfrak{s}}J_{1,n}^{\mathfrak{p}}H_{2,n}&0\\0&E_n^{\mathfrak{p}}J_{1,n}^{\mathfrak{s}}H_{2,n}\end{bmatrix}+\begin{bmatrix}E_n^{\mathfrak{s}}E_n^{\mathfrak{p}}H_{2,n}H_{2,n}&0\\0&E_n^{\mathfrak{p}}E_n^{\mathfrak{s}}H_{2,n}H_{2,n}\end{bmatrix},$$

$$\mathcal{J}_{2,n}=\begin{bmatrix}\widetilde{J}_{2,n}^{\mathfrak{p}}H_{2,n}&0\\0&\widetilde{J}_{2,n}^{\mathfrak{s}}H_{2,n}\end{bmatrix},\quad\mathcal{J}_{3,n}=\frac{\kappa_{\mathfrak{p}}^2+\kappa_{\mathfrak{s}}^2}{8\pi^2}|z'|^2\begin{bmatrix}\widetilde{S}_{0,n}\widetilde{J}_{3,n}&0\\0&\widetilde{S}_{0,n}\widetilde{J}_{3,n}\end{bmatrix},$$

$$\mathcal{J}_{4,n}=\frac{\kappa_{\mathfrak{p}}^2+\kappa_{\mathfrak{s}}^2}{8\pi^2}|z'|^2\begin{bmatrix}\widetilde{S}_{0,n}\widetilde{J}_{4,n}&0\\0&\widetilde{S}_{0,n}\widetilde{J}_{4,n}\end{bmatrix},$$

where

$$\begin{aligned}(J_{1,n}^\sigma\psi)(t)=&\frac{\kappa_\sigma^2}{4\pi}\int_0^{2\pi}\ln\Big(4\sin^2\frac{t-\varsigma}{2}\Big)P_n\left\{\sin(t-\cdot)\Big(|z'(\cdot)|^2-|z'(t)|^2\Big)\psi\right\}(\varsigma)\,\mathrm{d}\varsigma\\&+\frac{\mathrm{i}\kappa_\sigma^2}{2\pi}\int_0^{2\pi}P_n\left\{\Big(|z'(\cdot)|^2-|z'(t)|^2\Big)\psi\right\}(\varsigma)\,\mathrm{d}\varsigma,\\(\widetilde{J}_{2,n}^\sigma\psi)(t)=&\frac{\kappa_\sigma^2}{2\pi}\int_0^{2\pi}P_n\left\{(\cot\frac{t-\cdot}{2}+\mathrm{i})\Big(|z'(\cdot)|^2-|z'(t)|^2\Big)\psi\right\}(\varsigma)\,\mathrm{d}\varsigma,\\(\widetilde{J}_{3,n}\psi)(t)=&\int_0^{2\pi}P_n\left\{\cot\frac{t-\cdot}{2}\sin(t-\cdot)\psi\right\}(\varsigma)\,\mathrm{d}\varsigma,\\(\widetilde{J}_{4,n}\psi)(t)=&\int_0^{2\pi}\ln\Big(4\sin^2\frac{t-\varsigma}{2}\Big)P_n\Big\{(\cos(t-\cdot)-1)\psi\Big\}(\varsigma)\,\mathrm{d}\varsigma.\end{aligned}$$

Clearly, $\mathcal{S}_{0,n}\mathcal{S}_{0,n}\widetilde{\varphi}^n=\mathcal{S}_0\mathcal{S}_0\widetilde{\varphi}^n$, $\mathcal{H}_n\widetilde{\varphi}^n=\mathcal{H}\widetilde{\varphi}^n$ for $\widetilde{\varphi}^n\in X_n^2$.

In the following, we show the convergence of the full-discrete collocation method (4.5). To this end, we rewrite the function $\mathcal{B}\varphi$ in form of

$$(\mathcal{B}\varphi)(t) = \int_0^{2\pi} \ln\Big(4\sin^2\frac{t-\varsigma}{2}\Big)M(t,\varsigma)\varphi(\varsigma)\,\mathrm{d}\varsigma + \int_0^{2\pi} N(t,\varsigma)\varphi(\varsigma)\,\mathrm{d}\varsigma,$$

where

$$M(t,\varsigma) = \begin{bmatrix} m_1(t,\varsigma) & m_2(t,\varsigma) \\ m_3(t,\varsigma) & m_4(t,\varsigma) \end{bmatrix}, \qquad N(t,\varsigma) = \begin{bmatrix} n_1(t,\varsigma) & n_2(t,\varsigma) \\ n_3(t,\varsigma) & n_4(t,\varsigma) \end{bmatrix}.$$

Noting (3.12) and the analyticity of $k_j^\sigma(t,\varsigma), j = 1,2$, $\widetilde{h}_2^\sigma(t,\varsigma)$, $\widetilde{h}_3^\sigma(t,\varsigma)$ and the kernel of $\widetilde{H}_1$, we conclude that $m_j(t,t) = \partial_t m_j(t,t) = 0, j = 1,2,3,4$ and m_j, n_j are analytic. Recall that the full discretization of $\mathcal{B}$ is $\mathcal{B}_n = \mathcal{B}_{1,n} + \mathcal{B}_{2,n} + \mathcal{B}_{3,n}$.

Theorem 4.2. *Assume that $0 \le q \le p$ and $p > 1/2$. Then for the quadrature operator $\mathcal{B}_n$, the following estimates hold:*

$$\|\mathcal{B}_n\varphi - \mathcal{B}\varphi\|_{q+2} \le C\frac{1}{n^{p+1-q}}\|\varphi\|_p, \quad \|\mathcal{B}_n\chi - \mathcal{B}\chi\|_{q+2} \le \widetilde{C}\frac{1}{n^{p-q}}\|\chi\|_p \tag{4.6}$$

for all trigonometric polynomials $\varphi \in X_n^2$ and all $\chi \in H^p[0,2\pi]^2$, where C and $\widetilde{C}$ are positive constants depending on p and q.

Proof. For the derivative $\frac{\mathrm{d}}{\mathrm{d}t}(\mathcal{B}\varphi)$, it can be written in form of

$$(\mathcal{B}'\varphi)(t) \stackrel{\text{def}}{=} \frac{\mathrm{d}}{\mathrm{d}t}(\mathcal{B}\varphi)(t) = \int_0^{2\pi} \ln\Big(4\sin^2\frac{t-\varsigma}{2}\Big)\widetilde{M}(t,\varsigma)\varphi(\varsigma)\,\mathrm{d}\varsigma + \int_0^{2\pi} \widetilde{N}(t,\varsigma)\varphi(\varsigma)\,\mathrm{d}\varsigma,$$

where

$$\widetilde{M}(t,\varsigma) = \begin{bmatrix} \partial_t m_1(t,\varsigma) & \partial_t m_2(t,\varsigma) \\ \partial_t m_3(t,\varsigma) & \partial_t m_4(t,\varsigma) \end{bmatrix},$$
$$\widetilde{N}(t,\varsigma) = M(t,\varsigma)\cot\frac{t-\varsigma}{2} + \begin{bmatrix} \partial_t n_1(t,\varsigma) & \partial_t n_2(t,\varsigma) \\ \partial_t n_3(t,\varsigma) & \partial_t n_4(t,\varsigma) \end{bmatrix}.$$

We denote the full discretization of $\mathcal{B}'$ via interpolatory quadrature by

$$(\mathcal{B}_n'\varphi)(t) = \int_0^{2\pi} \ln\Big(4\sin^2\frac{t-\varsigma}{2}\Big)\mathcal{P}_n\Big\{\widetilde{M}(t,\cdot)\varphi\Big\}(\varsigma)\,\mathrm{d}\varsigma + \int_0^{2\pi} \mathcal{P}_n\Big\{\widetilde{N}(t,\cdot)\varphi\Big\}(\varsigma)\,\mathrm{d}\varsigma.$$

For $p > 1/2$ and the integer q satisfying $0 \le q \le p$, from $\widetilde{M}(t,t) = 0$ together with the analyticity of the elements in $\widetilde{M}(t,\varsigma)$ and $\widetilde{N}(t,\varsigma)$, using [17, Lemma 13.21 and Theorem 12.18], we have

$$\|\mathcal{B}_n'\varphi - \mathcal{B}'\varphi\|_{q+1} \le C_1\frac{1}{n^{p+1-q}}\|\varphi\|_p, \quad \|\mathcal{B}_n'\chi - \mathcal{B}'\chi\|_{q+1} \le \widetilde{C}_1\frac{1}{n^{p-q}}\|\chi\|_p$$

for all trigonometric polynomials $\varphi \in X_n^2$, where C_1 and $\widetilde{C}_1$ are positive constants depending on p and q. By $\mathcal{B}_n'\varphi = \frac{\mathrm{d}}{\mathrm{d}t}(\mathcal{B}_n\varphi)$, the above equation implies

$$\|\mathcal{B}_n\varphi - \mathcal{B}\varphi\|_{q+2} \le C_2\frac{1}{n^{p+1-q}}\|\varphi\|_p, \quad \|\mathcal{B}_n\chi - \mathcal{B}\chi\|_{q+2} \le \widetilde{C}_2\frac{1}{n^{p-q}}\|\chi\|_p$$

for some constants C_2, $\widetilde{C}_2$ depending on p and q. It follows from [17, Theorem 8.13] that the above inequality holds for arbitrary q satisfying $0 \le q \le p$ and $p > 1/2$, which completes the proof. □

Hereafter, the notation $a \lesssim b$ means $a \le Cb$, where $C > 0$ is a constant depending on p.

Theorem 4.3. *Assume that $p > 1/2$. Then for the quadrature operator $\mathcal{K}_n$, the following estimate holds:*

$$\|\mathcal{P}_n[\mathcal{E}_n^{-1}\mathcal{K}_n - \mathcal{E}^{-1}\mathcal{K}]\varphi\|_{p+2} \lesssim \frac{1}{n}\|\varphi\|_p$$

for all trigonometric polynomials $\varphi \in X_n^2$.

Proof. From Theorem 3.2 and the estimate (4.3), $\forall \chi \in H^p[0,2\pi]^2$, we have

$$\|(\mathcal{H}_n - \mathcal{H})\chi\|_{q,*} = \|\mathcal{H}(\mathcal{P}_n\chi - \chi)\|_{q,*} \le C_1\|(\mathcal{P}_n\chi - \chi)\|_q \le \frac{C_2}{n^{p-q}}\|\chi\|_p$$

for $0 \le q \le p$, $p \ge 1/2$, where C_1 is a positive constant depending on q and C_2 is a positive constant depending on p and q. Then, $\mathcal{H}_n$ and $\mathcal{H}_n - \mathcal{H}$ are uniformly bounded from $H^p[0,2\pi]^2$ to $H_*^p[0,2\pi]^2$ for $p \ge 1/2$. Clearly, $\mathcal{E}_n^{-1}\chi = \mathcal{E}^{-1}\chi$.

For all trigonometric polynomials $\varphi \in X_n^2$ of the form (4.2), using Theorem 4.2 and the fact that $\mathcal{H}_n\varphi = \mathcal{H}\varphi$, we get

$$\begin{aligned}
&\|\mathcal{H}_n\mathcal{B}_n\varphi - \mathcal{H}\mathcal{B}\varphi\|_{p+2} \le \|\mathcal{H}_n\mathcal{B}_n\varphi - \mathcal{H}\mathcal{B}\varphi\|_{p+2,*}\\
\le&\|\mathcal{H}_n(\mathcal{B}_n - \mathcal{B})\varphi\|_{p+2,*} + \|(\mathcal{H}_n - \mathcal{H})(\mathcal{B}\varphi - \mathcal{P}_n\mathcal{B}\varphi)\|_{p+2,*} + \|(\mathcal{H}_n - \mathcal{H})\mathcal{P}_n\mathcal{B}\varphi\|_{p+2,*}\\
\lesssim&\|(\mathcal{B}_n - \mathcal{B})\varphi\|_{p+2} + \|\mathcal{B}\varphi - \mathcal{P}_n\mathcal{B}\varphi\|_{p+2}\\
\lesssim&\frac{1}{n}\|\varphi\|_p + \frac{1}{n}\|\mathcal{B}\varphi\|_{p+3} \lesssim \frac{1}{n}\|\varphi\|_p.
\end{aligned}$$

Furthermore, it follows from Theorem 4.2 that $\mathcal{B}_n$ and $\mathcal{B}_n - \mathcal{B}$ are uniformly bounded from $H^p[0,2\pi]^2$ to $H^{p+2}[0,2\pi]^2$ for $p \ge 1/2$. Thus, using (4.3), (4.6) and the uniform boundedness of $\mathcal{P}_n : H^{p+2}[0,2\pi]^2 \to H^{p+2}[0,2\pi]^2$, together with the boundedness of $\mathcal{B} : H^p[0,2\pi]^2 \to H^{p+3}[0,2\pi]^2$, we deduce

$$\begin{aligned}
&\|\mathcal{B}_n^2\varphi - \mathcal{B}^2\varphi\|_{p+2} \le \|\mathcal{B}_n^2\varphi - \mathcal{B}^2\varphi\|_{p+4}\\
\le&\|\mathcal{B}_n(\mathcal{B}_n - \mathcal{B})\varphi\|_{p+4} + \|(\mathcal{B}_n - \mathcal{B})(\mathcal{B}\varphi - \mathcal{P}_n\mathcal{B}\varphi)\|_{p+4} + \|(\mathcal{B}_n - \mathcal{B})\mathcal{P}_n\mathcal{B}\varphi\|_{p+4}\\
\lesssim&\|(\mathcal{B}_n - \mathcal{B})\varphi\|_{p+2} + \|(\mathcal{B}\varphi - \mathcal{P}_n\mathcal{B}\varphi)\|_{p+2} + \frac{1}{n}\|\mathcal{P}_n\mathcal{B}\varphi\|_{p+2}\\
\lesssim&\frac{1}{n}\|\varphi\|_p + \frac{1}{n}\|\mathcal{B}\varphi\|_{p+3} + \frac{1}{n}\|\mathcal{B}\varphi\|_{p+2} \lesssim \frac{1}{n}\|\varphi\|_p.
\end{aligned}$$

Noting $\mathcal{H}_1\varphi \in X_n^2$, we obtain

$$\begin{aligned}
&\|\mathcal{B}_n\mathcal{H}_n\varphi - \mathcal{B}\mathcal{H}\varphi\|_{p+2} = \|(\mathcal{B}_n - \mathcal{B})\mathcal{H}\varphi\|_{p+2}\\
\le&\|(\mathcal{B}_n - \mathcal{B})(\mathcal{H}\varphi - \mathcal{P}_n\mathcal{H}\varphi)\|_{p+2} + \|(\mathcal{B}_n - \mathcal{B})\mathcal{P}_n\mathcal{H}\varphi\|_{p+2}\\
\lesssim&\|\mathcal{H}\varphi - \mathcal{P}_n\mathcal{H}\varphi\|_p + \frac{1}{n}\|\mathcal{P}_n\mathcal{H}\varphi\|_p\\
\le&\|\mathcal{H}_1\varphi - \mathcal{P}_n\mathcal{H}_1\varphi\|_p + \|\mathcal{H}_2\varphi - \mathcal{P}_n\mathcal{H}_2\varphi\|_p + \frac{1}{n}\|\mathcal{P}_n\mathcal{H}\varphi\|_p\\
\lesssim&\frac{1}{n^2}\|\mathcal{H}_2\varphi\|_{p+2} + \frac{1}{n}\|\mathcal{H}\varphi\|_p \lesssim \frac{1}{n}\|\varphi\|_p.
\end{aligned}$$

Therefore

$$\begin{aligned}
\|\mathcal{K}_n\varphi - \mathcal{K}\varphi\|_{p+2} \le&\|\mathcal{H}_n\mathcal{B}_n\varphi - \mathcal{H}\mathcal{B}\varphi\|_{p+2} + \|\mathcal{B}_n\mathcal{H}_n\varphi - \mathcal{B}\mathcal{H}\varphi\|_{p+2} + \|\mathcal{B}_n^2\varphi - \mathcal{B}^2\varphi\|_{p+2}\\
\lesssim&\frac{1}{n}\|\varphi\|_p.
\end{aligned}$$

The proof is completed by using the uniform boundedness of the operators $\mathcal{E}^{-1}, \mathcal{P}_n : H^{p+2}[0,2\pi]^2 \to H^{p+2}[0,2\pi]^2$. □

Theorem 4.4. *Assume that $p > 1/2$. Then for the quadrature operator $\mathcal{J}_n$, the following estimate holds:*

$$\|\mathcal{P}_n[\mathcal{E}_n^{-1}\mathcal{J}_n - \mathcal{E}^{-1}\mathcal{J}]\varphi\|_{p+2} \lesssim \frac{1}{n}\|\varphi\|_p$$

for all trigonometric polynomials $\varphi \in X_n^2$.

Proof. For all trigonometric polynomials $\varphi \in X_n^2$, we claim that

$$\|\mathcal{J}_n\varphi - \mathcal{J}\varphi\|_{p+2} \lesssim \frac{1}{n}\|\varphi\|_p.$$

In fact, analogous to the discussion in Theorem 4.2, we get

$$\begin{aligned}
\|J_{1,n}^\sigma\psi - J_1^\sigma\psi\|_{q+2} &\le C\frac{1}{n^{p+1-q}}\|\psi\|_p, \qquad 0 \le q \le p, \quad \frac{1}{2} < p,\\
\|\widetilde{J}_{4,n}\psi - \widetilde{J}_4\psi\|_{q+2} &\le C\frac{1}{n^{p+1-q}}\|\psi\|_p, \qquad 0 \le q \le p, \quad \frac{1}{2} < p,
\end{aligned}$$

for all trigonometric polynomials $\psi \in X_n$ and some constant C depending on p and q. Since $E_n^\sigma\varphi_j = E^\sigma\varphi_j$, $H_{2,n}\varphi_j = H_2\varphi_j \in X_n$, $j = 1, 2$, we have

$$\begin{aligned}
&\|\mathcal{J}_{1,n}\varphi - \mathcal{J}_1\varphi\|_{p+2}\\
=&\|(E_n^{\mathfrak{s}}J_{1,n}^{\mathfrak{p}}H_{2,n} - E^{\mathfrak{s}}J_1^{\mathfrak{p}}H_2)\varphi_1\|_{p+2} + \|(E_n^{\mathfrak{p}}J_{1,n}^{\mathfrak{s}}H_{2,n} - E^{\mathfrak{p}}J_1^{\mathfrak{s}}H_2)\varphi_2\|_{p+2}\\
\lesssim&\|(J_{1,n}^{\mathfrak{p}} - J_1^{\mathfrak{p}})H_2\varphi_1\|_{p+2} + \|(J_{1,n}^{\mathfrak{s}} - J_1^{\mathfrak{s}})H_2\varphi_2\|_{p+2}\\
\le&\|(J_{1,n}^{\mathfrak{p}} - J_1^{\mathfrak{p}})H_2\varphi_1\|_{p+4} + \|(J_{1,n}^{\mathfrak{s}} - J_1^{\mathfrak{s}})H_2\varphi_2\|_{p+4}\\
\lesssim&\frac{1}{n}\|H_2\varphi_1\|_{p+2} + \frac{1}{n}\|H_2\varphi_2\|_{p+2} \lesssim \frac{1}{n}\|\varphi\|_p.
\end{aligned}$$

Since the operator $\widetilde{J}_2^\sigma$ has an analytic kernel, it is easy to see

$$\|\mathcal{J}_{2,n}\varphi - \mathcal{J}_2\varphi\|_{p+2} \lesssim \frac{1}{n}\|\varphi\|_p.$$

In addition, in terms of $\widetilde{S}_{0,n}\psi = \widetilde{S}_0\psi$ for $\psi \in X_n$ and the uniform boundedness of $\widetilde{S}_{0,n}$ and $\widetilde{S}_{0,n} - \widetilde{S}_0$ from $H^p[0, 2\pi]^2$ to $H^{p+1}[0, 2\pi]^2$ for $p \ge 1/2$, we obtain

$$\begin{aligned}
&\|\mathcal{J}_{4,n}\varphi - \mathcal{J}_4\varphi\|_{p+2}\\
=&\frac{1}{8\pi^2}\sum_{j=1}^{2}\left\|\left((E_n^{\mathfrak{p}} + E_n^{\mathfrak{s}})\widetilde{S}_{0,n}\widetilde{J}_{4,n} - (E^{\mathfrak{p}} + E^{\mathfrak{s}})\widetilde{S}_0\widetilde{J}_4\right)\varphi_j\right\|_{p+2}\\
\le&\sum_{j=1}^{2}\left(\|\widetilde{S}_{0,n}(\widetilde{J}_{4,n} - \widetilde{J}_4)\varphi_j\|_{p+2} + \|(\widetilde{S}_{0,n} - \widetilde{S}_0)(\widetilde{J}_4\varphi_j - P_n\widetilde{J}_4\varphi_j)\|_{p+2}\right)\\
\le&\sum_{j=1}^{2}\left(\|\widetilde{S}_{0,n}(\widetilde{J}_{4,n} - \widetilde{J}_4)\varphi_j\|_{p+3} + \|(\widetilde{S}_{0,n} - \widetilde{S}_0)(\widetilde{J}_4\varphi_j - P_n\widetilde{J}_4\varphi_j)\|_{p+3}\right)\\
\lesssim&\sum_{j=1}^{2}\left(\|(\widetilde{J}_{4,n} - \widetilde{J}_4)\varphi_j\|_{p+2} + \|(\widetilde{J}_4\varphi_j - P_n\widetilde{J}_4\varphi_j)\|_{p+2}\right)\\
\lesssim&\sum_{j=1}^{2}\left(\frac{1}{n}\|\varphi_j\|_{p+2} + \frac{1}{n}\|(\widetilde{J}_4\varphi_j\|_{p+3}\right) \lesssim \frac{1}{n}\|\varphi\|_p.
\end{aligned}$$

Since the operator $\widetilde{J}_3$ has an analytic kernel, similarly we get

$$\|\mathcal{J}_{3,n}\varphi - \mathcal{J}_3\varphi\|_{p+2} \lesssim \frac{1}{n}\|\varphi\|_p.$$

Hence, the assertion of the theorem follows by using the uniform boundedness of the operators $\mathcal{E}^{-1}, \mathcal{P}_n : H^{p+2}[0,2\pi]^2 \to H^{p+2}[0,2\pi]^2$. □

Theorem 4.5. *For sufficiently large n, the approximate equation* (4.5) *is uniquely solvable and the solution satisfies the error estimate*

$$\begin{aligned}&\|\widetilde{\varphi}^n - \varphi\|_p\\ \le& L\Big\{\|\mathcal{P}_n\mathcal{S}_0\mathcal{S}_0\varphi - \mathcal{S}_0\mathcal{S}_0\varphi\|_{p+2} + \|\mathcal{P}_n[\mathcal{E}_n^{-1}(\mathcal{J}_n+\mathcal{K}_n) - \mathcal{E}^{-1}(\mathcal{J}+\mathcal{K})]\varphi\|_{p+2}\\ &+ \|\mathcal{P}_n[\mathcal{E}_n^{-1}\mathcal{A}_n - \mathcal{E}^{-1}\mathcal{A}]w\|_{p+2}\Big\},\end{aligned} \tag{4.7}$$

where L is a positive constant.

Proof. For all trigonometric polynomials $\varphi \in X_n^2$, it follows from Theorems 4.3 and 4.4 that

$$\|\mathcal{P}_n[\mathcal{E}_n^{-1}(\mathcal{J}_n+\mathcal{K}_n) - \mathcal{E}^{-1}(\mathcal{J}+\mathcal{K})]\varphi\|_{p+2} \lesssim \frac{1}{n}\|\varphi\|_p \to 0, \qquad n\to\infty$$

for all $p > 1/2$. Moreover, it is easy to see the estimates for $\|(J_{1,n}^\sigma - J_1^\sigma)\psi\|_{p+2}$ and $\|(\widetilde{J}_{4,n} - \widetilde{J}_4)\psi\|_{p+2}$ are valid analogously as (4.6). Then, we can obtain the uniform boundedness of the operator $\mathcal{P}_n[\mathcal{E}_n^{-1}(\mathcal{J}_n+\mathcal{K}_n) - \mathcal{E}^{-1}(\mathcal{J}+\mathcal{K})] : H^p[0,2\pi]^2 \to H^{p+2}[0,2\pi]^2$ from the proofs of Theorems 4.3 and 4.4. By the Banach–Steinhaus theorem (cf. [17, Problem 10.1]), we get the pointwise convergence

$$\mathcal{P}_n[\mathcal{E}_n^{-1}(\mathcal{J}_n+\mathcal{K}_n)]\varphi \to \mathcal{P}_n[\mathcal{E}^{-1}(\mathcal{J}+\mathcal{K})]\varphi \quad \text{as} \quad n\to\infty$$

for all $\varphi \in H^p[0,2\pi]^2$.

Hence (4.7) follows by employing [17, Corollary 13.13], $\mathcal{E}_n^{-1} = \mathcal{E}^{-1}$ and the uniform boundedness of the operators $\mathcal{E}_n^{-1}, \mathcal{P}_n : H^{p+2}[0,2\pi]^2 \to H^{p+2}[0,2\pi]^2$. □

The above theorem implies that the full-discrete collocation method (4.5) converges in $H^p[0,2\pi]^2$ for each $p > 1/2$.

5. Numerical experiments

In practice, instead of (4.5), we only need to solve the equivalent full-discrete equation of (3.4), i.e.,

$$\mathcal{P}_n\mathcal{H}_n\widetilde{\varphi}^n + \mathcal{P}_n\mathcal{B}_n\widetilde{\varphi}^n = \mathcal{P}_n w \;\Leftrightarrow\; A_n\widetilde{\varphi}^n = w^n, \tag{5.1}$$

where A_n is the coefficient matrix of the full-discrete equation. In fact, suppose that $\beta(t) = \frac{\kappa_{\mathrm{p}}^2+\kappa_s^2}{8\pi^2}|z'(t)|^2$, the equation (4.5) is equivalent to

$$\begin{aligned}&\mathcal{P}_n(\mathcal{S}_{0,n}\mathcal{S}_{0,n})\widetilde{\varphi}^n + \mathcal{P}_n[\beta^{-1}(\mathcal{J}_n+\mathcal{K}_n)\widetilde{\varphi}^n] = \mathcal{P}_n[\beta^{-1}\mathcal{A}_n w]\\ \Leftrightarrow\;& \mathcal{P}_n[\beta(\mathcal{S}_{0,n}\mathcal{S}_{0,n}\widetilde{\varphi}^n)] + \mathcal{P}_n[(\mathcal{J}_n+\mathcal{K}_n)\widetilde{\varphi}^n] = \mathcal{P}_n(\mathcal{A}_n w)\\ \Leftrightarrow\;& A_n^2\widetilde{\varphi}^n = A_n w^n.\end{aligned} \tag{5.2}$$

Since (4.5) is uniquely solvable by Theorem 4.5, it implies that the matrix A_n^2 is invertible, i.e., $\det A_n^2 = (\det A_n)^2 \neq 0$, and consequently A_n is invertible. Hence, (4.5) is equivalent to (5.1) by multiplying matrix A_n^{-1} on both ends of the equation (5.2). It is worth mentioning that the equivalent full-discrete equation (5.1) is

extremely efficient since it is formulated via simple quadrature operators $\mathcal{H}_n$ and $\mathcal{B}_n$.

For the smooth integrals, we simply use the trapezoidal rule

$$\int_0^{2\pi} f(\varsigma)\mathrm{d}\varsigma \approx \frac{\pi}{n}\sum_{j=0}^{2n-1} f(\varsigma_j^{(n)}).$$

For the singular integrals, we employ the following quadrature rules via the trigonometric interpolation:

$$\begin{aligned}
\int_0^{2\pi} \ln\Big(4\sin^2\frac{t-\varsigma}{2}\Big) f(\varsigma)\,\mathrm{d}\varsigma &\approx \sum_{j=0}^{2n-1} R_j^{(n)}(t) f(\varsigma_j^{(n)}),\\
\frac{1}{2\pi}\int_0^{2\pi} \cot\frac{\varsigma-t}{2} f(\varsigma)\,\mathrm{d}\varsigma &\approx \sum_{j=0}^{2n-1} U_j^{(n)}(t) f(\varsigma_j^{(n)}),\\
\int_0^{2\pi} \ln\Big(4\sin^2\frac{t-\varsigma}{2}\Big)\sin(t-\varsigma) f(\varsigma)\,\mathrm{d}\varsigma &\approx \sum_{j=0}^{2n-1} V_j^{(n)}(t) f(\varsigma_j^{(n)}),
\end{aligned} \tag{5.3}$$

where the quadrature weights are given by

$$\begin{aligned}
R_j^{(n)}(t) &= -\frac{2\pi}{n}\sum_{m=1}^{n-1}\frac{1}{m}\cos\Big[m(t-\varsigma_j^{(n)})\Big] - \frac{\pi}{n^2}\cos\Big[n(t-\varsigma_j^{(n)})\Big],\\
U_j^{(n)}(t) &= \frac{1}{2n}\big[1-\cos n(\varsigma_j^{(n)}-t)\big]\cot\frac{\varsigma_j^{(n)}-t}{2},\\
V_j^{(n)}(t) &= -\frac{\pi}{2n}\sin(\varsigma_j^{(n)}-t) + \frac{2\pi}{n}\sum_{m=2}^{n-1}\frac{\sin\Big[m(\varsigma_j^{(n)}-t)\Big]}{m^2-1} + \frac{2\pi\sin\Big[n(\varsigma_j^{(n)}-t)\Big]}{n(n^2-1)}.
\end{aligned}$$

Here, the weight $V_j^{(n)}$ is calculated by using [17, Lemma 8.23] and we also refer to [17] for the weights $R_j^{(n)}$ and $U_j^{(n)}$. On the other hand, the last items of $\mathcal{H}_{1,n}$ and $\mathcal{H}_{2,n}$ can be offset by the following item

$$\int_0^{2\pi} \mathcal{P}_n\left\{\begin{bmatrix} 0 & \widetilde{h}_3^{\mathfrak{s}}(t,\cdot)-h_3^{\mathfrak{s}}(t,\cdot)\\ \widetilde{h}_3^{\mathfrak{p}}(t,\cdot)-h_3^{\mathfrak{p}}(t,\cdot) & 0\end{bmatrix}\chi\right\}(\varsigma)\,\mathrm{d}\varsigma$$

in $\mathcal{B}_{2,n}$. Thus, the equation (5.1) becomes

$$\begin{aligned}
w_{1,i}^{(n)} &= -\varphi_{1,i}^{(n)} + \sum_{j=0}^{2n-1} X_{ij,\mathfrak{p}}^{(n)}\varphi_{1,j}^{(n)} + \sum_{j=0}^{2n-1} Y_{ij,\mathfrak{s}}^{(n)}\varphi_{2,j}^{(n)},\\
w_{2,i}^{(n)} &= \varphi_{2,i}^{(n)} + \sum_{j=0}^{2n-1} Y_{ij,\mathfrak{p}}^{(n)}\varphi_{1,j}^{(n)} - \sum_{j=0}^{2n-1} X_{ij,\mathfrak{s}}^{(n)}\varphi_{2,j}^{(n)},
\end{aligned} \tag{5.4}$$

TABLE 1. Parametrization of the exact boundary curves.

Type	Parametrization
Apple-shaped	$z(t) = \dfrac{0.55(1+0.9\cos t+0.1\sin 2t)}{1+0.75\cos t}(\cos t, \sin t), \quad t \in [0, 2\pi]$
Peach-shaped	$z(t) = 0.22(\cos^2 t\sqrt{1-\sin t}+2)(\cos t, \sin t), \quad t \in [0, 2\pi]$
Drop-shaped	$z(t) = (2\sin\dfrac{t}{2} - 1, -\sin t), \quad t \in [0, 2\pi]$
Heart-shaped	$z(t) = (\dfrac{3}{2}\sin\dfrac{3t}{2}, \sin t), \quad t \in [0, 2\pi]$

where $w_{l,i}^{(n)} = w_l(\varsigma_i^{(n)}), \varphi_{l,i}^{(n)} = \varphi_l(\varsigma_i^{(n)})$ for $i, j = 0, \cdots, 2n-1$, $l = 1, 2$, and

$$X_{ij,\sigma}^{(n)} = R_j^{(n)}(\varsigma_i^{(n)})k_1^\sigma(\varsigma_i^{(n)}, \varsigma_j^{(n)}) + \frac{\pi}{n}k_2^\sigma(\varsigma_i^{(n)}, \varsigma_j^{(n)}),$$

$$Y_{ij,\sigma}^{(n)} = U_j^{(n)}(\varsigma_i^{(n)}) + \frac{\kappa_\sigma^2}{4\pi}|z'(\varsigma_i^{(n)})|^2 V_j^{(n)}(\varsigma_i^{(n)}) + R_j^{(n)}(\varsigma_i^{(n)})\widetilde{h}_2^\sigma(\varsigma_i^{(n)}, \varsigma_j^{(n)}) + \frac{\pi}{n}h_3^\sigma(\varsigma_i^{(n)}, \varsigma_j^{(n)}) + \frac{\pi}{n}\widetilde{h}_1(\varsigma_i^{(n)}, \varsigma_j^{(n)}).$$

Remark 5.1. Moreover, a straightforward calculation yields

$$V_j^{(n)}(t) - R_j^{(n)}(t)\sin(t - \varsigma_j^{(n)}) = \frac{\pi\sin n(t-\varsigma_j^{(n)})}{n(n+1)} + \frac{\pi}{n^2}\sin n(t-\varsigma_j^{(n)})\cos(t-\varsigma_j^{(n)}),$$

which implies $V_j^{(n)}(\varsigma_i^{(n)}) - R_j^{(n)}(\varsigma_i^{(n)})\sin(\varsigma_i^{(n)} - \varsigma_j^{(n)}) = 0$. Therefore, $Y_{ij,\sigma}^{(n)}$ can be reduced to

$$Y_{ij,\sigma}^{(n)} = U_j^{(n)}(\varsigma_i^{(n)}) + R_j^{(n)}(\varsigma_i^{(n)})h_2^\sigma(\varsigma_i^{(n)}, \varsigma_j^{(n)}) + \frac{\pi}{n}h_3^\sigma(\varsigma_i^{(n)}, \varsigma_j^{(n)}) + \frac{\pi}{n}\widetilde{h}_1(\varsigma_i^{(n)}, \varsigma_j^{(n)}).$$

From this, we find that $E^\sigma H_2\varphi$ in (3.8) is only used for the theoretical analysis.

Remark 5.2. From [13, Section 4], we know that the trapezoidal rule and the quadrature formulas (5.3) yield convergence of an exponential order for a periodic analytic function f. In addition, from [17, Theorem 11.7], we conclude that our method has exponential convergence if the boundary of obstacle and the exact solution are analytic.

In the following, we show some numerical examples to demonstrate the superior performance of the proposed method. All of the numerical tests are implemented by using Matlab on a personal computer with a 64 GB RAM, 3.70 GHz Intel core i9 processor.

5.1. **Numerical examples: smooth obstacles.** We consider the elastic scattering by an apple-shaped and a peach-shaped obstacle with analytic and $\mathcal{C}^2$ boundary, respectively. The parametrizations of these two boundary curves are given in Theorem 1. To test the accuracy of the collocation method, we construct an exact solution by letting the exterior field of the elastic obstacle be generated by two point sources located at $\bar{x} = (0.1, 0.2)^\top \in D$, i.e.,

$$\phi_*(x) = H_0^{(1)}(\kappa_\mathfrak{p}|x-\bar{x}|), \quad \psi_*(x) = H_0^{(1)}(\kappa_\mathfrak{s}|x-\bar{x}|), \quad x \in \mathbb{R}^2 \setminus \overline{D}. \tag{5.5}$$

TABLE 2. Numerical errors for the apple-shaped and peach-shaped obstacles with $\omega = \pi$.

	Apple-shaped			Peach-shaped		
n	$\|\phi_* - \phi^{(n)}\|$	$\|\psi_* - \psi^{(n)}\|$	time	$\|\phi_* - \phi^{(n)}\|$	$\|\psi_* - \psi^{(n)}\|$	time
8	0.0677	0.0613	0.006s	0.0044	0.0050	0.007s
16	2.1192e-04	1.6939e-04	0.01s	3.9734e-04	4.5298e-04	0.01s
32	3.7880e-07	3.0432e-07	0.02s	5.4337e-05	6.1341e-05	0.02s
64	6.6341e-12	5.2998e-12	0.05s	6.9918e-06	7.8543e-06	0.05s
128	1.6200e-15	1.6162e-15	0.08s	8.8584e-07	9.9062e-07	0.08s
256	1.9389e-15	2.2955e-15	0.26s	1.1140e-07	1.2420e-07	0.28s
512	3.1540e-15	2.9617e-15	1.00s	1.3962e-08	1.5539e-08	1.08s
1024	4.2380e-15	3.7504e-15	4.25s	1.7475e-09	1.9429e-09	4.29s

TABLE 3. Numerical errors for the apple-shaped and peach-shaped obstacles with $\omega = 100\pi$.

	Apple-shaped			Peach-shaped		
n	$\|\phi_* - \phi^{(n)}\|$	$\|\psi_* - \psi^{(n)}\|$	time	$\|\phi_* - \phi^{(n)}\|$	$\|\psi_* - \psi^{(n)}\|$	time
64	2.2192	1.1012	0.05s	5.9298	2.5847	0.05s
128	7.2908e-02	9.2983e-02	0.08s	1.0250e-01	1.0459e-01	0.08s
256	5.5220e-07	1.0522e-06	0.27s	4.1347e-07	9.4716e-07	0.27s
512	6.0630e-13	4.4848e-13	1.06s	5.0089e-08	3.6659e-08	1.02s
1024	5.3276e-13	3.7980e-13	4.48s	6.2029e-09	4.3889e-09	4.42s
2048	4.8503e-13	4.0631e-13	16.39s	7.7281e-10	5.3866e-10	18.44s
4096	5.3277e-13	3.9049e-13	76.29s	9.6473e-11	6.6741e-11	76.27s

Due to the uniqueness of the boundary value problem (2.3), the solution can be constructed explicitly by enforcing the following boundary conditions on Γ_D:

$$f_1 = \partial_\nu \phi_* + \partial_\tau \psi_*, \qquad f_2 = \partial_\tau \phi_* - \partial_\nu \psi_*.$$

In numerical experiments, we take the Lamé parameters $\lambda = 3.88, \mu = 2.56$ and let the observation points be generated by $\{\varsigma_i^{(n)}\}_{i=0}^{2\tilde{n}-1}$, $\tilde{n} = 16$ and distributed on the circle $\partial B = \{x \in \mathbb{R}^2 : |x| = 3\}$. We list the numerical errors between the numerical solution and the corresponding exact solution with $L^2(\partial B)$ norm in Tables 2 and 3 for the angular frequency $\omega = \pi$ and $\omega = 100\pi$, respectively. It can be easily seen from the results that the accuracy is improved dramatically as the number of collocation points are increased. In fact, our method has an exponential convergence as the theoretical analysis suggests. We also find that the convergence rate of the apple-shaped obstacle with analytic boundary is faster than that of the peach-shaped obstacle with $\mathcal{C}^2$ boundary. The numerical solution and the corresponding exact solution are shown in Figure 1 for the apple-shaped obstacle. Clearly they coincide perfectly with $\omega = \pi, n = \tilde{n} = 16$.

For the high-frequency case, we can get the same highly accurate results as those of the low-frequency case by increasing the number of interpolation points. The numerical solution and the corresponding exact solution are shown in Figure 2 for the apple-shaped obstacle with $\omega = 100\pi$. As can be seen, the numerical solutions and the exact solutions also coincide perfectly when $n = \tilde{n} = 256$.

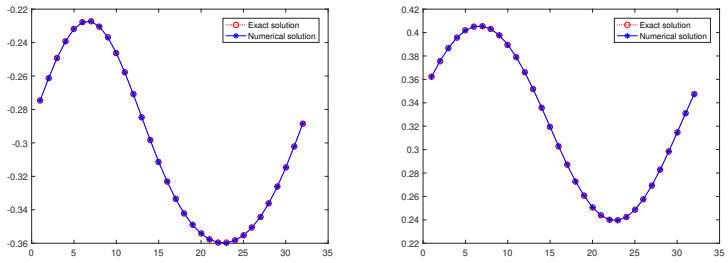

(a) $\Re(\phi)$ (b) $\Im(\phi)$

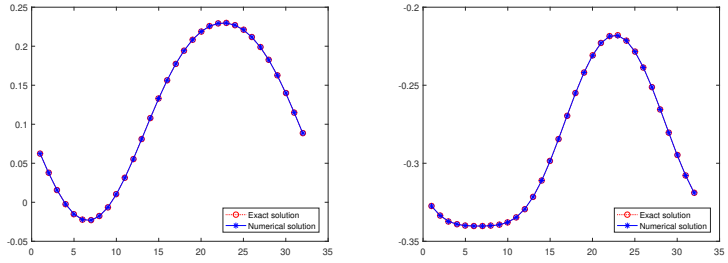

(c) $\Re(\psi)$ (d) $\Im(\psi)$

FIGURE 1. Numerical solutions and corresponding exact solutions for the apple-shaped obstacle with $\omega = \pi, n = \tilde{n} = 16$.

TABLE 4. Numerical errors for the drop-shaped domain with $\omega = \pi$.

	Point source			Plane wave		
n	$\|\phi_* - \phi^{(n)}\|$	$\|\psi_* - \psi^{(n)}\|$	time	$\|\phi^{(n_*)} - \phi^{(n)}\|$	$\|\psi^{(n_*)} - \psi^{(n)}\|$	time
16	2.0999e-03	2.1650e-03	0.01s	4.5396e-01	5.8469e-01	0.01s
32	2.4347e-08	3.1562e-08	0.03s	3.9571e-03	4.9919e-03	0.03s
64	1.2669e-08	1.6911e-08	0.07s	2.7795e-04	3.7244e-04	0.07s
128	3.8572e-10	5.1477e-10	0.09s	2.4339e-05	2.8050e-05	0.09s
256	1.1736e-11	1.5791e-11	0.31s	1.1917e-04	1.6019e-04	0.31s
512	1.3430e-14	1.7613e-14	1.14s	9.2866e-06	1.2593e-05	1.13s
1024	6.2155e-15	4.9608e-15	4.82s	5.5606e-06	7.5428e-06	4.77s
2048	6.1235e-15	5.9362e-15	17.52s	1.1380e-07	1.5203e-07	17.40s

It is worth mentioning that for a given incident wave and elastic obstacle, in view of (2.5) and (3.5), together with (5.4), we can get the compressional and shear far-field patterns immediately by using the trapezoidal rule. With the aid of (2.2), (3.1) and (5.4), noting $\boldsymbol{v}_{\mathfrak{p}} = \nabla\phi$ and $\boldsymbol{v}_{\mathfrak{s}} = \mathbf{curl}\psi$, we can also easily obtain the compressional and shear elastic scattered fields by using the trapezoidal rule, too, if the test points are not too close to the boundary.

5.2. **Numerical examples: nonsmooth obstacles.** In this subsection, we assume that D has a single corner at x_0 and $\Gamma_D \setminus \{x_0\}$ is analytic. The angle γ at the corner is assumed to satisfy $0 < \gamma < 2\pi$. Suppose that the corner point x_0

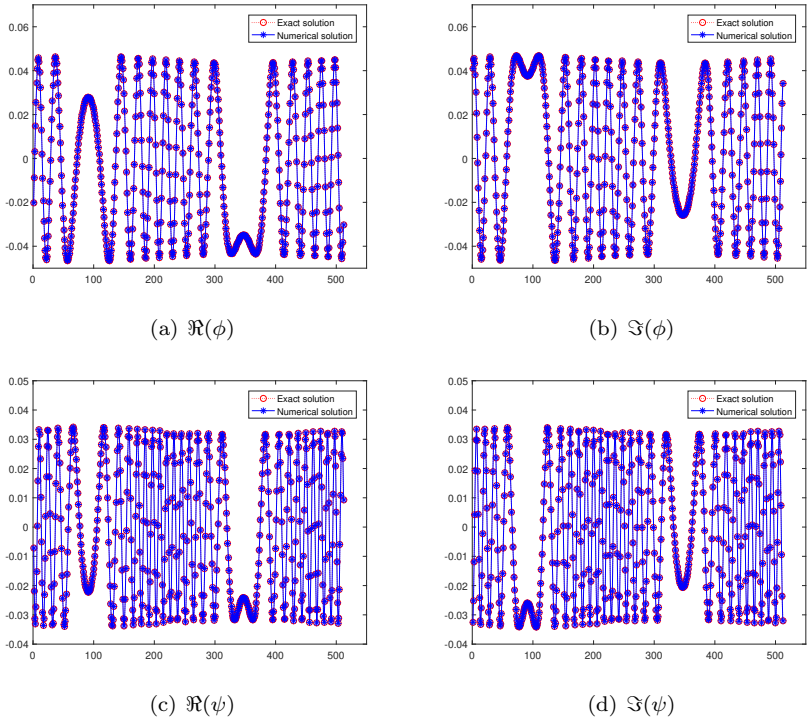

(a) $\Re(\phi)$ (b) $\Im(\phi)$

(c) $\Re(\psi)$ (d) $\Im(\psi)$

FIGURE 2. Numerical solutions and corresponding exact solutions for the apple-shaped obstacle with $\omega = 100\pi, n = \tilde{n} = 256$.

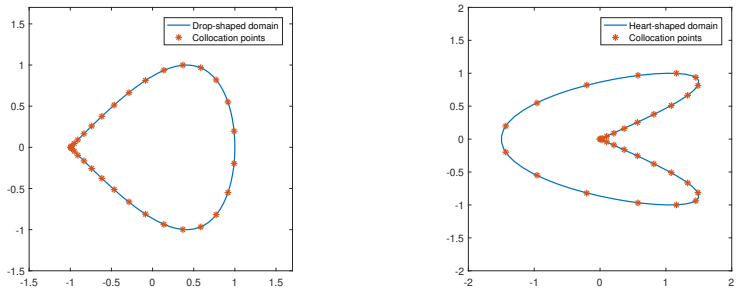

(a) $p = 2, n = 16$ (b) $p = 2, n = 16$

FIGURE 3. Collocation points on the drop-shaped and heart-shaped obstacles.

corresponds to the parameter $t = 0$ in the parametric representation of Γ_D. To test the accuracy of our method, we adopt the exact solutions in form of (5.5) with the point source located at $\bar{x} = (0.1, 0.2)^\top$ and $\bar{x} = (-0.5, 0.2)^\top$ for the drop-shaped and heart-shaped obstacles, respectively. The interior angles are $\gamma = \pi/2$

TABLE 5. Numerical errors for the heart-shaped domain with $\omega = \pi$.

	Point source			Plane wave		
n	$\|\phi_* - \phi^{(n)}\|$	$\|\psi_* - \psi^{(n)}\|$	time	$\|\phi^{(n_*)} - \phi^{(n)}\|$	$\|\psi^{(n_*)} - \psi^{(n)}\|$	time
16	4.3673e-02	1.0523e-01	0.02s	6.0929e-03	1.1896e-02	0.01s
32	6.0075e-04	1.5144e-03	0.03s	2.5014e-05	3.7337e-05	0.03s
64	4.3721e-07	8.4011e-07	0.07s	1.2432e-07	1.2820e-07	0.07s
128	1.8692e-09	1.2039e-09	0.09s	2.2355e-09	1.4398e-09	0.09s
256	1.1752e-11	7.5236e-12	0.31s	1.3571e-11	8.6880e-12	0.31s
512	1.6306e-13	1.0433e-13	1.17s	1.8443e-13	1.1843e-13	1.16s
1024	4.5946e-15	4.0851e-15	4.76s	8.0003e-15	5.9002e-15	4.82s
2048	1.1742e-14	1.3828e-14	17.84s	9.6079e-15	1.0804e-14	17.95s

and $\gamma = 3\pi/2$ for the drop-shaped and heart-shaped obstacles, respectively. The parameterizations of these two boundary curves are also shown in Table 1. In addition, we consider the case that the obstacle is illuminated by a compressional plane wave $\boldsymbol{u}^{\text{inc}}$ which is given by

$$\boldsymbol{u}^{\text{inc}}(x) = d\mathrm{e}^{\mathrm{i}\kappa_{\mathrm{p}} d\cdot x},$$

where $d = (\cos\theta, \sin\theta)^\top$ is the unit propagation direction vector.

To resolve the field near the corner, we adopt the graded mesh by taking the substitution $t = w(s)$ [7, 14], which is given by

$$w(s) = 2\pi \frac{[v(s)]^p}{[v(s)]^p + [v(2\pi - s)]^p}, \qquad 0 \le s \le 2\pi, \tag{5.6}$$

where

$$v(s) = \Big(\frac{1}{p} - \frac{1}{2}\Big)\Big(\frac{\pi - s}{\pi}\Big)^3 + \frac{1}{p}\frac{s - \pi}{\pi} + \frac{1}{2}, \qquad p \ge 2,$$

and is applied to the parametric curve of the drop-shaped and heart-shaped obstacles. In experiments, we choose $s_j := \pi j/n + \pi/(2n)$ as the collocation points. The generated points $w(s_j)$, $j = 0, \cdots, 2n-1$ of the graded mesh on the both boundaries are presented in Figure 3 for $p = 2$.

The numerical errors between the numerical solution and the exact solution (5.5) with $L^2(\partial B)$ norm for the drop-shaped and heart-shaped obstacles are listed in Tables 4 and 5 with the angular frequency $\omega = \pi$ and $\tilde{n} = 16$. Additionally, we calculate the values of compressional and shear scattered fields $\phi^{(n_*)}, \psi^{(n_*)}$ on ∂B with $\tilde{n} = 16, n_* = 4096$ by the incident plane wave with $\theta = \pi/6$, and compare them with the cases of other numbers of collocation points. For the point source case, the solver quickly converges to machine precision for both domains. This is due to the analyticity of the artificial solution. On the other hand, for the true scattering problem, i.e., the scattering problem of the plane wave incidence, we note that the numerical error of the heart-shaped domain is better than that of the drop-shaped domain. The reason is apparently related to the concavity of the domain. The detailed analysis will be investigated in a future work.

6. Extended cases

In this section, we consider the extension of the method to handle the Neumann problem and the three-dimensional problem.

6.1. **The Neumann problem.** We assume that the total field $\boldsymbol{u}$ satisfies the homogeneous Neumann boundary condition, i.e.,

$$T(\boldsymbol{u}) = 0 \quad \text{on } \Gamma_D, \tag{6.1}$$

where the traction operator T is defined by

$$T(\boldsymbol{u}) := 2\mu\partial_\nu \boldsymbol{u} + \lambda\nu\nabla\cdot\boldsymbol{u} - \mu\tau\mathrm{curl}\boldsymbol{u}.$$

Analogously, substituting the Helmholtz decomposition into (6.1) and taking the dot product with ν and τ respectively, we have the following coupled boundary value problem:

$$\begin{cases} \Delta\phi + \kappa_{\mathfrak{p}}^2\phi = 0, \quad \Delta\psi + \kappa_{\mathfrak{s}}^2\psi = 0, & \text{in } \mathbb{R}^2\setminus\overline{D}, \\ \mu\nu\cdot\partial_\nu\nabla\phi + \mu\nu\cdot\partial_\nu\mathbf{curl}\ \psi - \lambda\kappa_{\mathfrak{p}}^2\phi = f_1, & \text{on } \Gamma_D, \\ \mu\tau\cdot\partial_\nu\nabla\phi + \mu\tau\cdot\partial_\nu\mathbf{curl}\ \psi - \mu\kappa_{\mathfrak{s}}^2\psi = f_2, & \text{on } \Gamma_D, \\ \lim\limits_{\rho\to\infty}\rho^{\frac{1}{2}}(\partial_\rho\phi - \mathrm{i}\kappa_{\mathfrak{p}}\phi) = 0, \quad \lim\limits_{\rho\to\infty}\rho^{\frac{1}{2}}(\partial_\rho\psi - \mathrm{i}\kappa_{\mathfrak{s}}\psi) = 0, & \rho = |x|, \end{cases} \tag{6.2}$$

where

$$f_1 = -\nu\cdot T(\boldsymbol{u}^{\mathrm{inc}}), \quad f_2 = -\tau\cdot T(\boldsymbol{u}^{\mathrm{inc}}).$$

Furthermore, we assume that the solutions of (6.2) are in form of single-layer potentials as shown in (3.1). Letting $x\in\mathbb{R}^2\setminus\overline{D}$ tend to boundary Γ_D, using the new jump relations of the single-layer potentials recently derived in [9, Corollary 3.5] and the boundary conditions of (6.2), we obtain on Γ_D that

(6.3)

$$\begin{aligned} 2f_1(x) =& -\mu\kappa_{\mathfrak{p}}^2\nu^\top S^{\mathfrak{p}}\big[\nu\nu^\top g_1\big]\nu + \mu\nu^\top K^{\mathfrak{p}}\big[\tau\partial_\tau g_1 + g_1\partial_\tau\tau\big] - \mu\nu^\top H^{\mathfrak{p}}\big[\nu\partial_\tau g_1 + g_1\partial_\tau\nu\big] \\ &+ \mu\kappa_{\mathfrak{s}}^2\nu^\top S^{\mathfrak{s}}\big[\tau\nu^\top g_2\big]\nu + \mu\nu^\top K^{\mathfrak{s}}\big[\nu\partial_\tau g_2 + g_2\partial_\tau\nu\big] + \mu\nu^\top H^{\mathfrak{s}}\big[\tau\partial_\tau g_2 + g_2\partial_\tau\tau\big] \\ &- \lambda\kappa_{\mathfrak{p}}^2 S^{\mathfrak{p}}[g_1] - \mu(\nu\cdot\partial_\tau\tau)g_1 - \mu(\nu\cdot\partial_\tau\nu)g_2 - \mu\partial_\tau g_2, \\ 2f_2(x) =& -\mu\kappa_{\mathfrak{p}}^2\tau^\top S^{\mathfrak{p}}\big[\nu\nu^\top g_1\big]\nu + \mu\tau^\top K^{\mathfrak{p}}\big[\tau\partial_\tau g_1 + g_1\partial_\tau\tau\big] - \mu\tau^\top H^{\mathfrak{p}}\big[\nu\partial_\tau g_1 + g_1\partial_\tau\nu\big] \\ &+ \mu\kappa_{\mathfrak{s}}^2\tau^\top S^{\mathfrak{s}}\big[\tau\nu^\top g_2\big]\nu + \mu\tau^\top K^{\mathfrak{s}}\big[\nu\partial_\tau g_2 + g_2\partial_\tau\nu\big] + \mu\tau^\top H^{\mathfrak{s}}\big[\tau\partial_\tau g_2 + g_2\partial_\tau\tau\big] \\ &- \mu\kappa_{\mathfrak{s}}^2 S^{\mathfrak{s}}[g_2] - \mu(\tau\cdot\partial_\tau\tau)g_1 - \mu\partial_\tau g_1 - \mu(\tau\cdot\partial_\tau\nu)g_2. \end{aligned}$$

We point out that ν and τ inside of $[\cdot]$ are given with respect to the variable y, and are taken with respect to the variable x otherwise. As shown in [9, Section 5.2], we employ the quadrature formulas (5.3)–(5.8) of [9], then a Nyström-type discrete scheme can be achieved analogously.

TABLE 6. Numerical errors for the apple-shaped and peach-shaped obstacles with the Neumann boundary condition.

	Kite-shaped for $\omega = 3$		Kite-shaped for $\omega = 5$	
n	$\|\boldsymbol{v}_* - \boldsymbol{v}_{\boldsymbol{h}}\|_{(L^2(\Gamma_D))^2}$	time	$\|\boldsymbol{v}_* - \boldsymbol{v}_{\boldsymbol{h}}\|_{(L^2(\Gamma_D))^2}$	time
16	0.0717	0.01s	0.0883	0.01s
32	4.1975e-05	0.04s	1.2759e-04	0.04s
64	2.0601e-10	0.13s	7.6337e-10	0.13s
128	8.3623e-12	0.17s	1.2185e-11	0.17s
256	1.7041e-11	0.52s	8.7805e-11	0.54s
512	6.2898e-11	2.10s	2.2158e-10	2.12s

For comparison, we take the exact solutions in form of

$$\phi_*(x) = -H_0^{(1)}(\kappa_{\mathfrak{p}}|x|), \quad \psi_*(x) = 0, \quad x \in \mathbb{R}^2 \setminus \overline{D}, \tag{6.4}$$

as those in Example 2 of [5], i.e., $\boldsymbol{v_*} = \boldsymbol{\nabla}\phi_*$. We take the Lamé parameters $\lambda = 2, \mu = 1$ and let the observation points be generated by $\{\varsigma_i^{(n)}\}_{i=0}^{2\tilde{n}-1}$, $\tilde{n} = 16$ and distributed on the boundary Γ_D. Then, the numerical solution $\boldsymbol{v_h}$ on Γ_D can be described by

$$\boldsymbol{v_h} = \frac{1}{2}(-g_1 + K^{\mathfrak{p}} g_1 + H^{\mathfrak{s}} g_2)\nu + \frac{1}{2}(g_2 + H^{\mathfrak{p}} g_1 - K^{\mathfrak{s}} g_2)\tau. \tag{6.5}$$

We list the numerical errors $\|\boldsymbol{v_*} - \boldsymbol{v_h}\|_{(L^2(\Gamma_D))^2}$ in Table 6 for the angular frequency $\omega = 3$ and 5. It can be seen that for the Neumann problem, this method also has an exponential convergence as compared to only an algebraic convergence in [5] for the kite-shaped obstacle. Note that our accuracy stops at 11 digits due to the round-off errors in the singular kernel evaluation.

6.2. **The three-dimensional problem.** In three dimensions, the scattered field $\boldsymbol{v}$ satisfies the boundary value problem

$$\begin{cases} \mu\Delta\boldsymbol{v} + (\lambda+\mu)\boldsymbol{\nabla}\boldsymbol{\nabla}\cdot\boldsymbol{v} + \omega^2\boldsymbol{v} = 0 & \text{in } \mathbb{R}^3 \setminus \overline{D}, \\ \boldsymbol{v} = -\boldsymbol{u^i} & \text{on } \Gamma_D. \end{cases} \tag{6.6}$$

In addition, the scattered field $\boldsymbol{v}$ is required to satisfy the Kupradze–Sommerfeld radiation condition

$$\lim_{\rho\to\infty} \rho(\partial_\rho \boldsymbol{v}_{\mathfrak{p}} - \mathrm{i}\kappa_{\mathfrak{p}}\boldsymbol{v}_{\mathfrak{p}}) = 0, \quad \lim_{\rho\to\infty} \rho(\partial_\rho \boldsymbol{v}_{\mathfrak{s}} - \mathrm{i}\kappa_{\mathfrak{s}}\boldsymbol{v}_{\mathfrak{s}}) = 0, \quad \rho = |x|,$$

where

$$\boldsymbol{v}_{\mathfrak{p}} = -\frac{1}{\kappa_{\mathfrak{p}}^2}\nabla\nabla\cdot\boldsymbol{v}, \quad \boldsymbol{v}_{\mathfrak{s}} = \frac{1}{\kappa_{\mathfrak{s}}^2}\mathbf{curlcurl}\boldsymbol{v}.$$

For any solution $\boldsymbol{v}$ of the elastic wave equation, the Helmholtz decomposition reads

$$\boldsymbol{v} = \boldsymbol{\nabla}\phi + \mathbf{curl}\boldsymbol{\psi}, \quad \boldsymbol{\nabla}\cdot\boldsymbol{\psi} = 0. \tag{6.7}$$

Substituting (6.7) into (6.6) and taking the dot and cross products with the unit normal vector ν on Γ_D, respectively, we get the following coupled boundary value problem:

$$\begin{cases} \Delta\phi + \kappa_{\mathfrak{p}}^2\phi = 0, \quad \mathbf{curlcurl}\boldsymbol{\psi} - \kappa_{\mathfrak{s}}^2\boldsymbol{\psi} = 0 & \text{in } \mathbb{R}^3 \setminus \overline{D}, \\ \partial_\nu\phi + \nu\cdot\mathbf{curl}\boldsymbol{\psi} = \widetilde{f}_1, & \text{on } \Gamma_D, \\ \nu\times\boldsymbol{\nabla}\phi + \nu\times\mathbf{curl}\boldsymbol{\psi} = \widetilde{\boldsymbol{f}}_{\boldsymbol{2}}, & \text{on } \Gamma_D, \\ \lim\limits_{\rho\to\infty}\rho(\partial_\rho\phi - \mathrm{i}\kappa_{\mathfrak{p}}\phi) = 0, \quad \lim\limits_{\rho\to\infty}\rho(\mathbf{curl}\boldsymbol{\psi}\times\hat{x} - \mathrm{i}\kappa_{\mathfrak{s}}\boldsymbol{\psi}) = 0, & \rho = |x|, \end{cases} \tag{6.8}$$

where

$$\widetilde{f}_1 := -\nu\cdot\boldsymbol{u^i}, \quad \widetilde{\boldsymbol{f}}_{\boldsymbol{2}} := -\nu\times\boldsymbol{u^i}.$$

We assume that the solutions of (2.3) are given as

$$\begin{aligned} \phi(x) &= \int_{\Gamma_D} \Phi(x,y;\kappa_{\mathfrak{p}}) g_1(y)\,\mathrm{d}s(y), \qquad x \in \mathbb{R}^3 \setminus \Gamma_D \\ \boldsymbol{\psi}(x) &= \frac{1}{\kappa_{\mathfrak{s}}^2}\mathbf{curlcurl}\int_{\Gamma_D} \Phi(x,y;\kappa_{\mathfrak{s}})\boldsymbol{g_2}(y)\,\mathrm{d}s(y), \qquad x \in \mathbb{R}^3 \setminus \Gamma_D, \end{aligned} \tag{6.9}$$

where $g_1, \boldsymbol{g_2}$ are unknown densities and $\boldsymbol{g_2}$ satisfies $\boldsymbol{g_2} \cdot \nu = 0$, and

$$\Phi(x, y; \kappa_\sigma) = \frac{\exp(i\kappa_{\mathfrak{p}}|x - \bar{x}|)}{4\pi|x - \bar{x}|}, \quad \sigma = \mathfrak{p} \text{ or } \mathfrak{s}$$

is the fundamental solution for the three-dimensional Helmholtz equation. Letting $x \in \mathbb{R}^3 \setminus \overline{D}$ approach the boundary Γ_D in (6.9) and using the jump relations, we obtain the boundary integral equations

$$\begin{aligned} \widetilde{f}_1(x) &= -\frac{1}{2} g_1(x) + \int_{\Gamma_D} \frac{\partial \Phi(x, y; \kappa_{\mathfrak{p}})}{\partial \nu(x)} g_1(y)\, \mathrm{d}s(y) \\ &\qquad + \int_{\Gamma_D} \nu(x) \times \boldsymbol{\nabla}_x \Phi(x, y; \kappa_{\mathfrak{s}}) \cdot \boldsymbol{g_2}(y)\, \mathrm{d}s(y), \\ \widetilde{\boldsymbol{f_2}}(x) &= \int_{\Gamma_D} \nu(x) \times \boldsymbol{\nabla}_x \Phi(x, y; \kappa_{\mathfrak{p}}) g_1(y)\, \mathrm{d}s(y) \\ &\qquad + \frac{1}{2} \boldsymbol{g_2}(x) + \nu(x) \times \mathbf{curl} \int_{\Gamma_D} \Phi(x, y; \kappa_{\mathfrak{s}}) \boldsymbol{g_2}(y)\, \mathrm{d}s(y). \end{aligned} \tag{6.10}$$

For numerical purpose, we test the formulation on two three-dimensional objects, which are both axis-symmetric. More specifically, they are generated by rotating curves in the xz plane with respect to the z axis. One object is a sphere with the generating curve given by

$$x = 2\cos(s), \quad z = 2\sin(s), \quad -\pi/2 \le s \le \pi/2.$$

Another one is an ellipsoid by rotating the curve

$$x = \cos(s), \quad z = 2\sin(s), \quad -\pi/2 \le s \le \pi/2.$$

Since the high order evaluation of singular kernels is sophisticated in three dimensions, we only show the numerical results and will report the detailed implementation in a forthcoming paper. We refer to [20] for some general ideas.

TABLE 7. Numerical errors for the elastic scattering of three dimensional objects with the Dirichlet boundary condition.

	Sphere			Ellipsoid		
n	$\|\phi_* - \phi^{(n)}\|$	$\|\psi_* - \psi^{(n)}\|$	time	$\|\phi_* - \phi^{(n)}\|$	$\|\psi_* - \psi^{(n)}\|$	time
16	9.398e-08	4.7368e-08	0.46s	1.9535e-03	1.3936e-03	0.65s
32	1.0760e-08	4.4180e-09	0.96s	9.2980e-03	4.7679e-03	1.01s
64	6.9880e-08	2.9426e-09	1.75s	2.3378e-05	1.4425e-05	1.81s
96	1.2475e-08	4.8461e-09	3.09s	5.5093e-06	3.4974e-06	3.02s
128	1.4175e-08	2.8216e-09	4.50s	1.4484e-06	1.8909e-06	4.34s
256	1.2361e-08	1.9374e-09	16.55s	1.9392e-09	3.5646e-10	16.28s
320	6.4661e-10	3.1789e-10	23.79s	5.2607e-12	7.5933e-13	24.54s

To verify the accuracy, we replace $\phi_*(x)$ and $\psi_*(x)$ in (5.5) by their three dimensional counterparts and still use them to generate the exact solution. The source is located at $(0.2, 0.2, 0.2)$. The angular frequency is $\omega = \pi$ and the Lamé parameters are $\lambda = 3.88$, $\mu = 2.56$. Numerical results are presented in Table 7 and Figure 4. Note that in Table 7, n is the number of discretization points along the generating curve. One can see that the spectral accuracy is achieved by adding more discretization points.

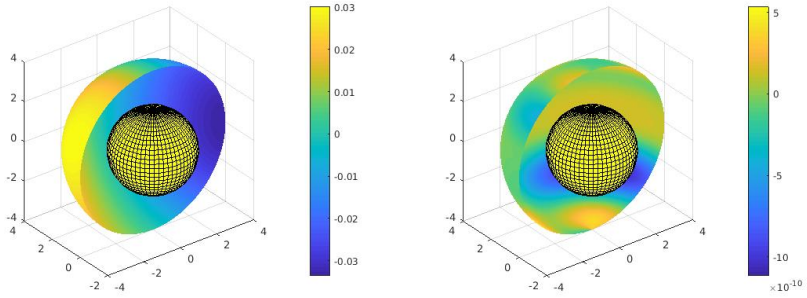

(a) (b)

FIGURE 4. Elastic scattering of a sphere: (a) the real part of the first component of $\boldsymbol{v}$; (b) the error compared to the exact solution.

7. Conclusion

We have proposed a novel boundary integral formulation and developed a highly accurate numerical method for solving the time-harmonic elastic scattering by a rigid bounded obstacle immersed in a homogeneous and isotropic elastic medium. Using the Helmholtz decomposition, we reduce the scattering problem to a coupled boundary integral equation with singular integral operators. By introducing an appropriate requlatizer to the coupled system, we split the operator equation into an isomorphic operator plus a compact one. The convergence is shown for both the semi-discrete and full-discrete schemes via the collocation method. Numerical experiments for smooth and nonsmooth obstacles, especially for the obstacles with corners, are presented to demonstrate the superior performance of the proposed method. Furthermore, we extend this numerical method to the Neumann problem and the three-dimensional elastic obstacle scattering problem. Future work includes the application of the method for solving the inverse elastic scattering problems and the multiple elastic scattering problems.

References

[1] J. F. Ahner and G. C. Hsiao, *On the two-dimensional exterior boundary-value problems of elasticity*, SIAM J. Appl. Math., **31** (1976), 677–685.
[2] B. Alpert, *Hybrid Gauss-trapezoidal quadrature rules*, SIAM J. Sci. Comput., **20** (1999) 1551–1584.
[3] H. Ammari, E. Bretin, J. Garnier, H. Kang, H. Lee, and A. Wahab, *Mathematical Methods in Elasticity Imaging*, Princeton University Press, New Jersey, 2015.
[4] A. Anand, J. Ovall, and C. Turc, *Well conditioned boundary integral equations for two-dimensional sound-hard scattering problems in domains with corners*, J. Integral Equ. Appl., **24** (2012), 1–38.
[5] G. Bao, L. Xu, and T. Yin, *An accurate boundary element method for the exterior elastic scattering problem in two dimensions*, J. Comput. Phys., **348** (2017), 343–363.
[6] F. Bu, J. Lin, and F. Reitich, *A fast and high-order method for the three-dimensional elastic wave scattering problem*, J. Comput. Phys., **258** (2014), 856–870.
[7] D. Colton and R. Kress, *Inverse Acoustic and Electromagnetic Scattering Theory*, 3rd edition, Springer, New York, 2013.
[8] H. Dong, J. Lai, and P. Li, *Inverse obstacle scattering for elastic waves with phased or phaseless far-field data*, SIAM J. Imaging Sci., **12** (2019), 809–838.

[9] H. Dong, J. Lai, and P. Li, *An inverse acoustic-elastic interaction problem with phased or phaseless far-field data*, Inverse Probl., **36** (2020), 035014.
[10] L. Greengard and S. Jiang, *A new mixed potential representation for the equations of unsteady, incompressible flow*, SIAM Review, **61** (2019), 733–755.
[11] G. Hu, A. Kirsch, and M. Sini, *Some inverse problems arising from elastic scattering by rigid obstacles*, Inverse Probl., **29** (2013), 015009
[12] A. Kirsch, *An Introduction to the Mathematical Theory of Inverse Problems*, 2nd edition, Springer, New York, 2011.
[13] A. Kirsch and S. Ritter, *The Nyström method for solving a class of singular integral equations and applications in 3D-plate elasticity*, Math. Meth. Appl. Sci., **22** (1999), 177–197.
[14] R. Kress, *A Nyström method for boundary integral equations in domains with corners*, Numer. Math., **58** (1990), 145–161.
[15] R. Kress, *On the numerical solution of a hypersingular integral equation in scattering theory*, J. Comput. Appl. Math., **61** (1995), 345–360.
[16] R. Kress, *A collocation method for a hypersingular boundary integral equation via trigonometric differentiation*, J. Integral Equ. Appl., **26** (2014), 197–213.
[17] R. Kress, *Linear Integral Equations*, 3rd edition, Springer, New York, 2014.
[18] R. Kress and I. H. Sloan, *On the numerical solution of a logarithmic integral equation of the first kind for the Helmholtz equation*, Numer. Math., **66** (1993), 199–214.
[19] J. Lai and P. Li, *A framework for simulation of multiple elastic scattering in two dimensions*, SIAM J. Sci. Comput., **41** (2019), A3276–A3299.
[20] J. Lai, and M. O'Neil, *An FFT-accelerated direct solver for electromagnetic scattering from penetrable axisymmetric objects*, J. Comput. Phys., **390** (2019), 152–174.
[21] L. D. Landau and E. M. Lifshitz, *Theory of Elasticity*, Oxford: Pergamon 1986.
[22] F. Le Louër, *On the Fréchet derivative in elastic obstacle scattering*, SIAM J. Appl. Math., **72** (2012), 1493–1507.
[23] F. Le Louër, *A high order spectral algorithm for elastic obstacle scattering in three dimensions*, J. Comput. Phys., **279** (2014), 1–17.
[24] S. G. Mikhlin and S. Prössdorf, *Singular Integral Operators*, Springer Verlag, Berlin, 1986.
[25] Y. H. Pao and V. Varatharajulu, *Huygens' principle, radiation conditions, and integral formulas for the scattering of elastic waves*, J. Acoust. Soc. Amer., **59** (1976), 1361–1371.
[26] J. Saranen and G. Vainikko, *Trigonometric collocation methods with product integration for boundary integral equations on closed curves*, SIAM J. Numer. Anal., **33** (1996), 1577–1596.
[27] M. S. Tong and W. C. Chew, *Nyström method for elastic wave scattering by three-dimensional obstacles*, J. Comput. Phys., **226** (2007), 1845–1858.
[28] Y. Wang, A. S. Leonov, D. V. Lukyanenko and A. G.Yagola, *General Tikhonov Regularization with Applications in Geoscience*, CSIAM Trans. Appl. Math., **1** (2020), 53–85.
[29] J. Yue, M. Li, P. Li, and X. Yuan, *Numerical solution of an inverse obstacle scattering problem for elastic waves via the Helmholtz decomposition*, Commun. Comput. Phys., **26** (2019), 809–837.

School of Mathematics, Jilin University, Changchun, Jilin 130012, China
Email address: dhp@jlu.edu.cn

School of Mathematical Sciences, Zhejiang University Hangzhou, Zhejiang 310027, China
Email address: laijun6@zju.edu.cn

Department of Mathematics, Purdue University, West Lafayette, Indiana 47907, USA
Email address: lipeijun@math.purdue.edu